The Journal of Immunology

Phenotypic Polarization of Activated Astrocytes: The Critical Role of Lipocalin-2 in the Classical Inflammatory Activation of Astrocytes

Eunha Jang, Jong-Heon Kim, Shinrye Lee, Jae-Hong Kim, Jung-Wan Seo, Myungwon Jin, Maan-Gee Lee, Il-Sung Jang, Won-Ha Lee and Kyoungho Suk

References This article **cites 80 articles**, 23 of which you can access for free at:
http://www.jimmunol.org/content/191/10/5204.full#ref-list-1

Why *The JI*? Submit online.

- **Rapid Reviews! 30 days*** from submission to initial decision

- **No Triage!** Every submission reviewed by practicing scientists

- **Fast Publication!** 4 weeks from acceptance to publication

*average

Subscription Information about subscribing to *The Journal of Immunology* is online at:
http://jimmunol.org/subscription

Permissions Submit copyright permission requests at:
http://www.aai.org/About/Publications/JI/copyright.html

Email Alerts Receive free email-alerts when new articles cite this article. Sign up at:
http://jimmunol.org/alerts

Phenotypic Polarization of Activated Astrocytes: The Critical Role of Lipocalin-2 in the Classical Inflammatory Activation of Astrocytes

Eunha Jang,* Jong-Heon Kim,* Shinrye Lee,*,[1] Jae-Hong Kim,* Jung-Wan Seo,* Myungwon Jin,* Maan-Gee Lee,* Il-Sung Jang,[†] Won-Ha Lee,[‡] and Kyoungho Suk*

Astrocytes provide structural and functional support for neurons, as well as display neurotoxic or neuroprotective phenotypes depending upon the presence of an immune or inflammatory microenvironment. This study was undertaken to characterize multiple phenotypes of activated astrocytes and to investigate the regulatory mechanisms involved. We report that activated astrocytes in culture exhibit two functional phenotypes with respect to pro- or anti-inflammatory gene expression, glial fibrillary acidic protein expression, and neurotoxic or neuroprotective activities. The two distinct functional phenotypes of astrocytes were also demonstrated in a mouse neuroinflammation model, which showed pro- or anti-inflammatory gene expression in astrocytes following challenge with classical or alternative activation stimuli; similar results were obtained in the absence of microglia. Subsequent studies involving recombinant lipocalin-2 (LCN2) protein treatment or *Lcn2*-deficient mice indicated that the pro- or anti-inflammatory functionally polarized phenotypes of astrocytes and their intracellular signaling pathway were critically regulated by LCN2 under in vitro and in vivo conditions. Astrocyte-derived LCN2 promoted classical proinflammatory activation of astrocytes but inhibited IL-4–STAT6 signaling, a canonical pathway involved in alternative anti-inflammatory activation. Our results suggest that the secreted protein LCN2 is an autocrine modulator of the functional polarization of astrocytes in the presence of immune or inflammatory stimuli and that LCN2 could be targeted therapeutically to dampen proinflammatory astrocytic activation and related pathologies in the CNS. *The Journal of Immunology*, 2013, 191: 5204–5219.

Astrocytes provide structural and functional support for neurons, release gliotransmitters to modulate synaptic activity, and participate in synapse formation and remodeling (1). Astrocytes also have an ability to respond to and participate in immune and inflammatory responses in the CNS (2, 3). Although the immune and inflammatory responses are a normal defense mechanism aimed at protecting the brain from infection, injury, cellular debris, or abnormal protein aggregation, excessive neuroinflammation has been implicated in diverse neurodegenerative diseases (4, 5). As an important regulator of brain inflammation,

activated astrocytes can release, in response to various stimuli, a wide array of immune and inflammatory mediators, such as pro- and anti-inflammatory cytokines/chemokines, which may subsequently exert neuroprotective or neurotoxic effects (6). Microglia, another glial cell type of mesodermal origin, also contribute to both neuroprotection and neurotoxicity (7); when activated in response to immune stimuli, they release pro- or anti-inflammatory cytokines/chemokines. These distinct patterns of microglial activation are referred to as functional polarization, which has implications in diverse CNS conditions, such as cerebral ischemia, Alzheimer's disease, and spinal cord injury (8–11). Although activated astrocytes can release pro- or anti-inflammatory mediators with neurotoxic or neuroprotective effects, the functional polarization of astrocytes and the regulation of their polarized phenotypes have not been clearly determined.

Lipocalin 2 (LCN2) has been implicated in diverse cellular processes, such as cell growth (12), cell death/survival (13, 14), cell migration/invasion (15), and cell differentiation (16). LCN2 was also shown to play an important role in iron delivery (13, 17), angiogenesis (18), febrile response (19), insulin resistance (20), and inflammation as an acute-phase protein (21). Recently, we (22) and other investigators (23–25) reported that brain glial cells express and secrete LCN2 under inflammatory conditions and that LCN2 mediates reactive astrocytosis (26). Nevertheless, the functional role of LCN2 in the CNS is far from clear.

Based on previously reported involvements of LCN2 in reactive astrocytosis under diverse CNS injury and disease conditions (27–32), we hypothesized that LCN2 may be a pivotal regulator of the functional phenotypes of activated astrocytes. Through a series of in vitro and in vivo experiments, we show that functional dichotomy, such as M1/M2 observed for microglia and macrophages, also exists in activated astrocytes and that LCN2 is an autocrine promoter of the classical proinflammatory activation of astrocytes.

*Department of Pharmacology, Brain Science and Engineering Institute, Cell and Matrix Research Institute, Kyungpook National University School of Medicine, Daegu 700-422, Korea; [†]Department of Pharmacology, Brain Science and Engineering Institute, Kyungpook National University School of Dentistry, Daegu 700-422, Korea; and [‡]School of Life Sciences and Biotechnology, Kyungpook National University, Daegu 702-701, Korea

[1]Current address: Department of Oral Microbiology, Kyungpook National University School of Dentistry, Daegu, Korea.

Address correspondence and reprint requests to Prof. Kyoungho Suk, Department of Pharmacology, Kyungpook National University School of Medicine, 680 Gukchaebosang Street, Joong-gu, Daegu 700-422, Republic of Korea. E-mail address: ksuk@knu.ac.kr.

The online version of this article contains supplemental material.

Abbreviations used in this article: ACM, astrocyte-conditioned media; ARG1, arginase 1; DI, discrimination index; GFAP, glial fibrillary acidic protein; Iba-1, ionized calcium-binding adapter molecule 1; IC, immune complex; i.c.v., intracerebroventricular(ly); iNOS, inducible NO synthase; KO, knockout; LCN2, lipocalin 2; WT, wild-type.

Materials and Methods

Reagents

The following chemicals were obtained from Sigma-Aldrich (St. Louis, MO): LPS from *Escherichia coli* 0111:B4 (prepared by phenolic extraction and gel filtration chromatography), H_2O_2, glutamate, leflunomide [5-methylisoxazole-4-(4-trifluoromethyl) carboxanilide; a STAT6 inhibitor], and OVA. Immune complexes (ICs) were made by mixing a 10-fold molar excess of rabbit anti-OVA IgG (Cappel, Durham, NC) with OVA for 30 min at room temperature. Recombinant mouse IL-4, mouse IL-10, mouse LCN2, and mouse IFN-γ were purchased from R&D Systems (Minneapolis, MN). Bacterially expressed recombinant mouse LCN2 protein was prepared as previously described (26). Briefly, recombinant mouse LCN2 protein was expressed as a GST fusion protein in *E. coli* BL21, which does not synthesize siderophore. The protein was purified using glutathione-Sepharose 4B beads (GE Healthcare, Princeton, NJ).

Cell cultures

Neonatal astrocyte cultures were prepared from mixed glia cultures, as previously described with minor modifications (26, 33). In brief, the whole brains of 2–3-d-old mice were chopped and mechanically disrupted using a nylon mesh. The cells obtained were seeded in culture flasks and grown at 37˚C in a 5% CO_2 atmosphere in DMEM supplemented with 10% FBS, 100 U/ml penicillin, and 100 μg/ml streptomycin (Life Technologies-BRL, Rockville, MD). Culture media were changed initially after 5 d and then changed every 3 d, and cells were used after culture for 14–21 d. Primary astrocytes were obtained by shaking mixed glial cultures at 250 rpm overnight. Culture media were discarded, and astrocytes were dissociated using trypsin-EDTA (Life Technologies-BRL) and then collected by centrifuging at $500 \times g$ for 10 min. Primary astrocyte cultures were grown and maintained in DMEM supplemented with 10% FBS and penicillin-streptomycin. The purities of astrocyte cultures exceeded 96%, as determined by glial fibrillary acidic protein (GFAP) staining and flow cytometry (Supplemental Fig. 1). Furthermore, to determine the degree of microglial contamination in the primary astrocyte cultures, traditional RT-PCR amplification of microglia or myeloid markers, such as ionized calcium-binding adapter molecule 1 (*Iba-1*), *Cx3cr1*, *F4/80*, *CD11c*, and *CD11d*, was carried out (Supplemental Fig. 1). Expression of these microglia or myeloid markers was not detected in the astrocyte cultures. Mixed glial cultures and microglia cultures were used as a positive control. Adult astrocytes were isolated from the whole brains of 12-wk-old mice, as previously described with some modifications (34). Briefly, mice were perfused with ice-cold saline, and brains were removed and placed in calcium- and magnesium-free ice-cold HBSS (Invitrogen, Carlsbad, CA). Meninges were removed, and brain tissues were chopped using a razor blade. Chopped tissues were digested in HBSS with 0.25% trypsin, 1 mM EDTA, and 0.04 mg/ml bovine pancreatic DNase I (Sigma-Aldrich) for 10 min at 37˚C and then centrifuged at $880 \times g$ for 10 min. Using a nylon mesh, digested tissues were mechanically disrupted and centrifuged at $500 \times g$ for 10 min. Supernatants were removed, and cell pellets were resuspended in HBSS. Suspensions of cell pellets in HBSS were carefully added to the top of a discontinuous Percoll density gradient (Amersham Biosciences, Piscataway, NJ) and centrifuged for 15 min at $1000 \times g$ at room temperature. The Percoll density gradient was prepared at 60, 30, 25, 20, and 15%. Astrocytes were collected from the 25% layer and from a portion of the 20% layer. Collected astrocytes were centrifuged for 5 min at $880 \times g$ and resuspended in sterile HBSS. The purity of primary adult astrocytes was >90%, as determined by GFAP staining (data not shown). Primary cultures of dissociated cerebral cortical neurons were prepared from embryonic day 20 mice, as described previously (35, 36). Briefly, mouse embryos were decapitated, and brains were rapidly removed and placed in a culture dish containing cold PBS. Cortices were isolated, transferred to a culture dish containing 0.25% trypsin-EDTA in PBS for 30 min at 37˚C, and washed twice in serum-free neurobasal media (Life Technologies-BRL). Cortical tissues were mechanically dissociated by gentle pipetting, and the dissociated cortical cells obtained were seeded onto plates coated with poly-D-lysine (Sigma-Aldrich) in neurobasal media containing 2 mM glutamine (Sigma-Aldrich), penicillin-streptomycin, nerve growth factor (Invitrogen), N2 supplement (Life Technologies-BRL), and B27 supplement (Life Technologies-BRL).

Astrocyte-conditioned media and astrocyte/neuron cocultures

To obtain astrocyte-conditioned media (ACM), primary astrocytes were plated at a density of 5×10^4 cells/well in 96-well plates and stimulated with LPS, IL-4, or IL-10 for 24 h. The cells were then washed with PBS and cultured in fresh DMEM for an additional 24 h, as previously described (37). Conditioned media were collected and centrifuged at $320 \times g$ for 2 min to remove cellular debris. ACM were added to cortical neurons plated at 5×10^4 cells/well in 96-well plates. Cortical neuron cells were incubated for 24 h, with or without glutamate or H_2O_2, before measuring viability. For astrocyte/neuron cocultures, cortical neurons were plated at a density of 2×10^5 cells/well in 24-well companion plates and allowed to settle at 37˚C in a 5% CO_2 atmosphere for 7 d. Primary astrocytes were plated separately at 2×10^5 cells/well in cell culture inserts (0.4 μm pore size) and allowed to settle at 37˚C in a 5% CO_2 atmosphere overnight. They were then treated with LPS, IL-4, or IL-10 for 24 h and washed. Cell culture inserts containing astrocytes were transferred to the wells containing cortical neurons and incubated for 24 h, and neuronal cell viabilities were measured.

Traditional and real-time RT-PCR

Total RNA was extracted from astrocytes cultured in six-well plates using TRIzol reagent (Invitrogen), according to the manufacturer's instructions. Reverse transcription was conducted using Superscript II (Invitrogen) and oligo(dT) primer. Traditional PCR amplification using specific primer sets was carried out at an annealing temperature of 55–60˚C over 20–30 cycles. PCR was performed using a DNA Engine Tetrad Peltier Thermal Cycler (MJ Research, Waltham, MA). To analyze PCR products, 10 μl each PCR reaction was electrophoresed on 1% agarose gel stained with ethidium bromide and detected under UV light. Real-time PCR was performed using the Perfect Real Time One Step SYBR PrimeScript RT-PCR Kit (Takara Bio, Shiga, Japan), followed by detection using the ABI Prism 7000 Sequence Detection System (Applied Biosystems, Foster City, CA). *Gapdh* was used as the internal control. The nucleotide sequences of the primers were based on published cDNA sequences (Table I).

Assessment of cell viability by MTT assay

Primary astrocyte and cortical neuron cultures were treated with various stimuli for specific times. After treatment, media were removed, and MTT (0.5 mg/ml; Sigma-Aldrich) was added and incubated at 37˚C for 3 h in a 5% CO_2 incubator. Insoluble formazan crystals were completely dissolved in DMSO, and absorbance at 570 nm was measured using a microplate reader (Anthos Labtec Instruments, Wals, Austria).

Nitrite quantification

Cells were stimulated in 96-well plates, and nitrite (NO_2^-) levels in culture media were measured using the Griess reaction, as previously described (26), to assess NO production levels. Samples (50 μl) were mixed with 50 μl Griess reagent (1% sulfanilamide/0.1% naphthylethylene diamine dihydrochloride/2% phosphoric acid) in 96-well plates and incubated at 25˚C for 10 min. Absorbances at 540 nm were measured using a microplate reader (Anthos Labtec Instruments), and $NaNO_2$ standards were used to calculate nitrite levels.

TNF-α, CXCL10, and LCN2 ELISA

The levels of TNF-α and CXCL10 in culture media were measured by sandwich ELISA using rat monoclonal anti-mouse TNF-α and CXCL10 Ab as capture Abs and goat biotinylated polyclonal anti-mouse TNF-α and CXCL10 Ab as detection Abs (ELISA development reagent; R&D Systems), as previously described (38, 39). Recombinant mouse TNF-α and CXCL10 protein (R&D Systems) were used as standards. The levels of LCN2 in culture media were measured by sandwich ELISA using a goat polyclonal anti-mouse LCN2 Ab (R&D Systems) as the capture Ab and rabbit polyclonal anti-mouse LCN2 Ab as a detection Ab (Santa Cruz Biotechnology, Santa Cruz, CA). The polyclonal anti-mouse LCN2 Ab was detected by sequential incubation with HRP-conjugated anti-rabbit IgG Ab (Pierce, Rockford, IL) and chromogenic substrates (R&D Systems). Recombinant mouse LCN2 protein was used as a standard.

Flow cytometric analysis

Primary astrocyte cultures (2×10^5) were pelleted, fixed, and incubated with primary Abs (goat polyclonal anti-arginase 1 [ARG1] Ab [Novus, Littleton, CO]; goat polyclonal anti-MRC1 Ab [R&D Systems]) for 20 min on ice. Cells were then washed twice and incubated with FITC-labeled secondary Ab (FITC-conjugated anti-goat IgG Ab; Millipore, Billerica, MA). Alternatively, astrocytes were incubated directly with Alexa Fluor 488–labeled rat anti-F4/80 Ab (Serotec, Oxford, U.K.) or Alexa Fluor 647–labeled mouse anti-GFAP Ab (BD Biosciences, San Jose, CA). Flow cytometric analysis was performed using a FACSCalibur flow cytometer (BD Biosciences). For background fluorescence, cells were stained with nonimmune goat IgG as a control Ab (Millipore). The fluorescence profiles of 1×10^4 cells were collected and analyzed. ARG1 expression was determined

after cell permeabilization using 90% ice-cold methanol by intracellular flow cytometry.

Western blot analysis

Cells were lysed in triple-detergent lysis buffer (50 mM Tris-HCl [pH 8], 150 mM NaCl, 0.02% sodium azide, 0.1% NaDodSO$_4$ [SDS], 1% Nonidet P-40, 0.5% sodium deoxycholate, and 1 mM PMSF). Protein concentrations in cell lysates were determined using a protein assay kit (Bio-Rad, Hercules, CA). Equal amounts of protein were separated by 12% SDS-PAGE and then transferred to Hybond ECL nitrocellulose membranes (Amersham Biosciences, Piscataway, NJ). Membranes were blocked with 5% skim milk, sequentially incubated with primary Abs (rabbit polyclonal anti-GFAP Ab, mouse monoclonal anti–α-tubulin [Sigma-Aldrich], rabbit polyclonal anti–phospho-STAT6 at Tyr[641] Ab [Cell Signaling Technology, Beverly, MA], rabbit polyclonal anti-total STAT6 Ab [Abcam, Cambridge, MA]) and HRP-conjugated secondary Abs (anti-rabbit and anti-mouse IgG Ab; Amersham Biosciences), and proteins were detected by ECL (Amersham Biosciences).

Mouse breeding and maintenance

Lcn2 knockout (KO) mice were generously donated by Dr. Kiyoshi Mori (Kyoto University, Kyoto, Japan) and by Dr. Shizuo Akira (Osaka University, Osaka, Japan). Wild-type (WT) and *Lcn2* KO mice were backcrossed for 8–10 generations in a C57BL/6 background to generate homozygous and heterozygous animals, as described previously (17, 40). Genotypes were confirmed by PCR of genomic DNA (40). Age- and sex-matched *Lcn2* WT and KO mice were used for all experiments. All animals used in this study were acquired and cared for in accordance with guidelines published by the National Institutes of Health for the care and use of laboratory animals. The study protocol was approved by the Institutional Review Board of Kyungpook National University School of Medicine.

Intracerebroventricular injection

Mice were anesthetized using an i.p. injection of a mixture of Zoletil (tiletamine/zolazepam) (Virbac, Carros, France) and Rompun (xylazine) (Bayer Pharma, Puteaux, France) at doses of 30 and 10 mg/kg, respectively, and secured in a stereotaxic instrument (Stoelting, Wood Dale, IL). One microliter of saline, LPS (5 μg), or IL-4 (100 ng) was injected intracerebroventricularly (i.c.v.), using a 5-μl Hamilton syringe, into lateral ventricles on both sides at the following coordinates: 0.5 mm posterior, 1 mm lateral to the bregma, and 1.75 mm below the skull surface at the point of entry.

The LPS neuroinflammatory model

A peripheral injection (i.p.) of LPS (5 mg/kg) was given to evoke neuroinflammation in mice, as previously described (41). Controls were administered an equivalent volume of saline i.p. Behavioral and mRNA analyses were conducted 24 h after injection.

Microglia/macrophage depletion

Mice were administered liposomal clodronate or control liposome (Clophosome; Formumax, Palo Alto, CA) to eliminate macrophages and brain-resident microglia (200 μl/mouse i.p. or 10 μl/mouse i.c.v., respectively) 72 h prior to IL-4 treatment (42, 43). Liposomal clodronate was injected both i.p. and i.c.v. to completely remove microglia, as well as macrophages.

Open-field test

Open-field testing was performed to assess LPS-induced reduction of motility (44). At 24 h after an i.p. injection of saline or LPS, mice were placed individually at the corner of an arena (40 × 40 × 40 cm; with white acrylic walls). After a 1-min adaptation period, animal behavior was recorded for 30 min using a digital camera fixed 2 m above the arena floor. Total distance traveled (cm) and speed (cm/s) were analyzed using a video-tracking system (Smart; Panlab, Barcelona, Spain). The arena was wiped between trials with 70% ethyl alcohol, and to minimize stress levels, tests were performed under a low-illumination red light.

Object-recognition task

Two objects were used: a metal cylinder (diameter 7 cm, height 10 cm) and a plastic rectangular cuboid filled with sand (5 × 5 × 10 cm). Mice were first habituated to the testing arena for 5 min in the absence of objects. During the training session, mice were exposed to two identical objects, which were placed in opposite corners of the arena ∼3 cm away from the walls, and allowed to explore them for 10 min. At 24 h after an i.p. injection of LPS, mice were replaced in the arena containing a familiar object in its previous location and a novel object in place of the object removed. The total time spent exploring each object was recorded for 10 min. Exploration was defined as being within 1 cm of an object or touching it with the nose. Objects were thoroughly cleaned between trials to remove any scents. Relative exploration time was measured using discrimination index (DI) = (time spent at the novel object − time spent at the familiar object)/(time spent at the novel object + time spent at the familiar object)]. Thus, a positive DI value indicates that mice spent more time exploring the novel object, whereas a DI of 0 indicates that mice spent equal time at the two objects.

Tail-suspension test

The tail-suspension test was performed as previously described (45). In brief, mice were suspended by the tail for 6 min using adhesive tape attached along the distal half of the tail in a closed white acrylic box. The free end of the tape was attached to a horizontal bar 35 cm above the floor. Total duration of immobility was recorded.

Immunohistochemistry

Mice were sacrificed 24–48 h after administering saline, LPS, or IL-4 by ether inhalation and subjected to intracardiac perfusion-fixation using a solution of 0.9% NaCl and 4% paraformaldehyde in 0.1 M PBS (pH 7.4). Isolated brains were immersion-fixed in 4% paraformaldehyde for 72 h. For cryoprotection, brains were incubated in 30% sucrose diluted in 0.1 M PBS for 72 h and embedded in OCT compound (Tissue-Tek; Sakura Finetek USA, Torrance, CA), and frozen sections were cut sagittally at 12 μm. Sections were permeabilized in 0.1% Triton X-100 and blocked with 1% BSA and 5% normal donkey serum for 1 h at room temperature. Sections were incubated with primary Abs (goat polyclonal anti-LCN2 [1:1000 dilution; R&D Systems], rabbit polyclonal anti-iNOS [1:200 dilution; BD Transduction Laboratories, Lexington, KY], goat polyclonal anti-ARG1 [1:500 dilution; Novus], mouse anti-GFAP [1:500 dilution; BD Biosciences], rabbit polyclonal anti-GFAP [1:500 dilution; DakoCytomation]) at 4°C overnight, followed by incubation for 1 h at room temperature with secondary Abs (Cy3-conjugated donkey anti-goat, rabbit IgG and FITC-conjugated donkey anti-mouse, or rabbit IgG Abs; Jackson ImmunoResearch). For some experiments, sections were incubated directly with Alexa Fluor 488–labeled anti-F4/80 Ab (1:500; Serotec). Sections were then mounted and counterstained using gelatin containing DAPI. Tiled images of each section were captured with a CCD color video camera (Olympus D70) through a 100× objective lens attached to a fluorescence microscope (Olympus BX51). Three squares (500 × 500 μm) were placed in the primary motor cortex or hippocampus in the subthreshold images of six independent sagittal sections. The cells in these three squares were counted and statistically analyzed, as previously described, using the NIH ImageJ program (46). Composite images of stained sections were filtered to eliminate low-frequency drift (>20 pixels = 50 μm) and high-frequency noise (<1 pixel). Images were binarily thresholded at 50% of the background level, and GFAP[+], iNOS[+], or ARG1^{+} cell particles were counted. For diaminobenzidine immunohistochemistry, the sections were incubated at 4°C overnight with rabbit polyclonal Iba-1 Ab (1:500 dilution; Wako, Tokyo, Japan) or rat monoclonal CD11b Ab (1:500 dilution; Serotec). The sections were then incubated with biotinylated anti-rabbit or anti-rat IgG Ab (1:200 dilution; Vector Laboratories, Burlingame, CA). Subsequently, the sections were incubated with avidin–biotin complex reagents (Vector Laboratories) for 30 min at room temperature, followed by detection with diaminobenzidine.

Statistical analyses

Data are presented as the mean ± SD of three or more independent experiments, unless stated otherwise. Statistical comparisons between treatments were made using the Student *t* test. The analysis was performed using SPSS version 14.0K (SPSS, Chicago, IL). Statistical significance was accepted for *p* values < 0.05.

Results

Classical or alternative activation of astrocytes in culture

To determine whether cultured astrocytes exhibit functionally polarized phenotypes, we evaluated the expression profiles of several genes in mouse neonatal astrocyte cultures following exposure to classical or alternative activation stimuli (Table I). In microglia and macrophages, LPS/IFN-γ induces classical activation, whereas IL-4, IC+LPS, and IL-10 induce three subsets of alternative activation status (47). After cultured astrocytes were treated with

Table I.   DNA sequences of the primers used for RT-PCR

Mouse cDNA	RT-PCR Method	Primer Sequences	GenBank Accession No.
Il-1β	Real-time	Forward, 5′-AAG TTG ACG GAC CCC AAA AGA T-3′ Reverse, 5′-TGT TGA TGT GCT GCT GCG A-3′	NM_008361
Inos	Real-time	Forward, 5′-GCC ACC AAC AAT GGC AAC A-3′ Reverse, 5′-CGT ACC GGA TGA GCT GTG AAT T-3′	NM_010927
Tnf-α	Real-time	Forward, 5′-ATG GCC TCC CTC TCA TCA GTT C-3′ Reverse, 5′-TTG TGG GTT TGC TAC GAC GTG-3′	NM_013693
Cxcl10	Real-time	Forward, 5′-AAG TGC TGC CGT CAT TTT CT-3′ Reverse, 5′-GTG GCA ATG ATC TCA ACA CG-3′	NM_021274
Il-12	Real-time	Forward, 5′-GCC CTC TCT CTC CTC TTG CT-3′ Reverse, 5′-GTC TGC CTC TTT TGG TCA GG-3′	NM_013652
Il-23	Real-time	Forward, 5′-CGA CTG TTG CCT CTC GTA CA-3′ Reverse, 5′-AGG AGG TTC ACA GCC CTT TT-3′	NM_016960
Il-10	Real-time	Forward, 5′-AGT GAA CTG CGC TGT CAA TG-3′ Reverse, 5′-TTC AGG GTC AAG GCA AAC TT-3′	NM_009140
Arg1	Real-time	Forward, 5′-CGC CTT TCT CAA AAG GAC AG-3′ Reverse, 5′-CCA GCT CTT CAT TGG CTT TC-3′	NM_007482
Mrc1	Real-time	Forward, 5′-TGG CTA CCA GGA AGT CCA TC-3′ Reverse, 5′-TGT AGC AGT GGC CTG CAT AG-3′	NM_008625
Il-1ra	Real-time	Forward, 5′-CCA GCT CAT TGC TGG GTA CT-3′ Reverse, 5′-TTC TCA GAG CGG ATG AAG GT-3′	NM_031167
Fizz1	Real-time	Forward, 5′-TCC CAG TGA ATA CTG ATG AGA-3′ Reverse, 5′-CCA CTC TGG ATC TCC CAA GA-3′	NM_020509
Ym1	Real-time	Forward, 5′-GGG CAT ACC TTT ATC CTG AG-3′ Reverse, 5′-CCA CTG AAG TCA TCC ATG TC-3′	NM_009892
Gfap	Traditional	Forward, 5′-AGG CAG AAG CTC CAA GAT GA-3′ Reverse, 5′-TGT GAG GTC TGC AAA CTT GG-3′	NM_034407
Lcn2	Real-Time	Forward, 5′-CCC CAT CTC TGC TCA CTG TC-3′ Reverse, 5′-TTT TTC TGG ACC GCA TTG-3′	NM_008491
Iba-1	Traditional	Forward, 5′- GAA GCG AAT GCT GGA GAA A -3′ Reverse, 5′- GAC CAG TTG GCC TCT TGT GT -3′	NM_019467
Cx3cr1	Traditional	Forward, 5′-CAC CAT TAG TCC TGG GCG GT CT-3′ Reverse, 5′-GAT GAG GAA GTA GCA AAA GC-3′	NM_009987
F4/80	Traditional	Forward, 5′-CTT TGG CTA TGG GCT TCC AGT C-3′ Reverse, 5′-GCA AGG AGG ACA GAG TTT ATC GTG-3′	NM_010130
CD11c	Traditional	Forward, 5′-CTG GAT AGC CTT TCT TCT GCT G-3′ Reverse, 5′-GCA CAC TGT GTC CGA ACT C-3′	NM_021334
CD11d	Traditional	Forward, 5′-TCA CTG CGA AAC AAT GAA GC-3′ Reverse, 5′-CTC AAA CGG GAA AGA AGC TG-3′	NM_001029872
24p3R	Traditional	Forward, 5′-AAT GAC TCT CAC GGG GAT TG-3′ Reverse, 5′-AGT GGT GGG GAT GAC TTC AG-3′	NM_021551
Megalin	Traditional	Forward, 5′-CCA GAA AAT GTG AAA AAC CAG-3′ Reverse, 5′-ACA AGG TTT GCG GTG TCT TT-3′	NM_001081088
Gapdh	Traditional	Forward, 5′-ACC ACA GTC CAT GCC ATC AC-3′ Reverse, 5′-TCC ACC ACC CTG TTG CTG TA-3′	NM_008084
Gapdh	Real-time	Forward, 5′-TGG GCT ACA CTG AGC ACC AG-3′ Reverse, 5′-GGG TGT CGC TGT TGA AGT CA-3′	NM_008084

GenBank Web site: http://www.ncbi.nlm.nih.gov/.

these stimuli, real-time RT-PCR analysis was conducted to determine the mRNA levels of individual pro- or anti-inflammatory genes previously associated with either classical (*Il-1β*, *Inos*, *Tnf-α*, *Cxcl10*, *Il-12*, and *Il-23*) or alternative (*Il-10*, *Arg1*, *Mrc1*, *Il-1ra*, *Fizz1*, and *Ym1*) activation (Fig. 1A). Representative phenotypic markers of classical (*Il-1β*, *Inos*, *Tnf-α*, and *Cxcl10*) or alternative (*Il-10*, *Arg1*, *Mrc1*, *Il-1ra*, *Fizz1*, and *Ym1*) activation were found to be strongly induced by the respective stimuli. LPS/IFN-γ stimulation induced most proinflammatory genes (*Il-1β*, *Inos*, *Tnf-α*, and *Cxcl10*), but it did not affect the expression of *Il-12*, *Il-23*, or anti-inflammatory genes. In contrast, alternative activation stimuli (IL-4, IC+LPS, or IL-10) did not have significant effects on proinflammatory genes, but they upregulated anti-inflammatory genes to different extents. IL-4 induced all alternative activation markers examined, whereas IC+LPS had no effect on the expression of these genes. IL-10 had a significant effect on *Arg1* and *Mrc1* only. Polarized classical versus alternative activation responses were also confirmed by the ratio of expressed markers (*Il-1β/Il-1ra*, *Inos/Arg1*, and *Tnf-α/Il-10*) (Fig. 1B). The ratio of classical/alternative activation markers was markedly in-

creased after LPS/IFN-γ treatment. We next evaluated NO production and the expression of some phenotypic markers at the protein level (Fig. 2). LPS/IFN-γ–activated astrocytes strongly induced classical activation–related NO production, TNF-α, and CXCL10 protein secretion (Fig. 2A). Flow cytometric analysis revealed that ARG1 and MRC1 protein expression was increased by IL-4 or IL-10 but not by IC+LPS (Fig. 2B). An increase in GFAP expression is a hallmark of reactive astrocytes. Furthermore, LPS/IFN-γ treatment was shown to induce changes in astrocytes that are similar to those that occur during reactive astrocytosis (48). The effects of LPS/IFN-γ or IL-4 on GFAP expression were evaluated by traditional RT-PCR and Western blot analysis. GFAP expression at both the mRNA and protein levels was increased by LPS/IFN-γ treatment, whereas IL-4 had no significant effect on GFAP expression (Fig. 2C, 2D), and it reduced LPS/IFN-γ–induced GFAP expression (data not shown). These results indicate that cultured astrocytes exhibit polarized phenotypes: those of classical and alternative activation. However, the nature of the phenotypic polarization of astrocytes might be different from those of microglia or macrophages. Furthermore, subtypes of alternative activation

FIGURE 1. Identification of phenotypic polarization in primary astrocyte cultures based on gene-expression profiles. Primary astrocyte cultures were treated with LPS (100 ng/ml) plus IFN-γ (50 U/ml), IL-4 (10 ng/ml), ICs (OVA [75 μg/ml] plus anti-OVA Ab [150 μg/ml]) plus LPS (100 ng/ml), or IL-10 (10 ng/ml) for 8 h, and total RNAs were isolated. (**A**) The mRNA levels of phenotypic markers (*Il-1β, Inos, Tnf-α, Cxcl10, Il-12, Il-23, Il-10, Arg1, Mrc1, Il-1ra, Fizz1,* and *Ym1*) were determined by real-time RT-PCR. (**B**) Polarized classical versus alternative activation was also assessed by the ratio of expressed mRNA markers (*Il-1β/Il-1ra, Inos/Arg1, Tnf-α /Il-10*). *Gapdh* was used as an internal control. Results are mean ± SD (*n* = 3). *$p < 0.05$, versus untreated control.
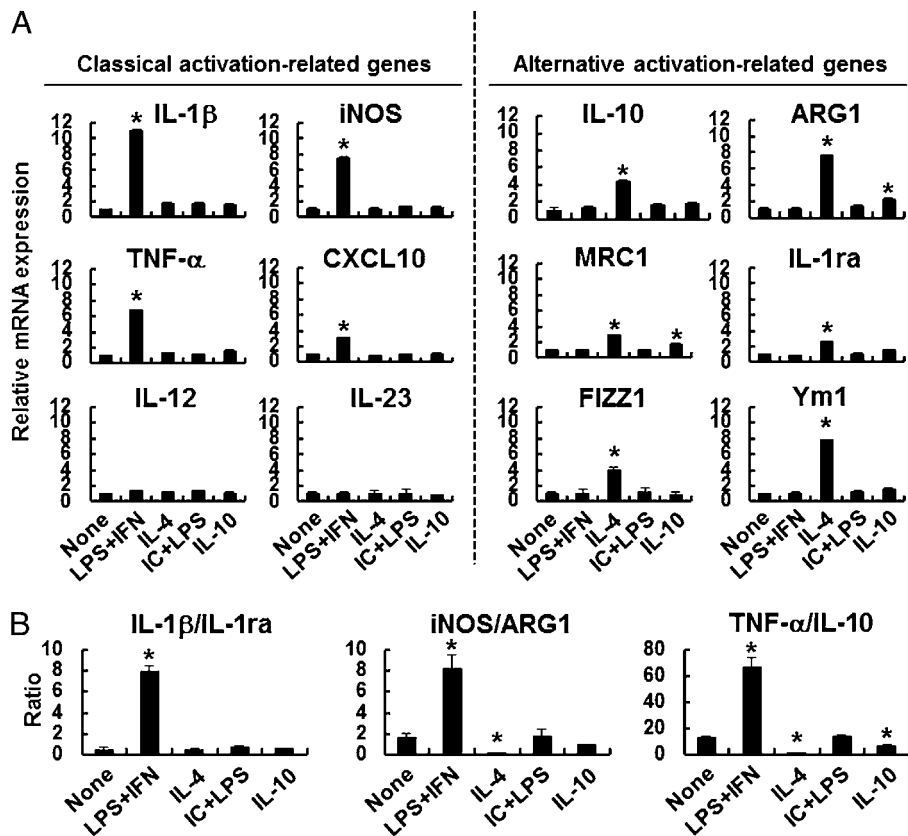
statuses, such as M2a, M2b, or M2c, may not be present in astrocytes or may not be as distinct in astrocytes as in microglia/macrophages.

Functional polarization of astrocytes in culture: neuroprotective versus neurotoxic phenotypes

Having found that astrocytes express the respective phenotypic markers following treatment with classical or alternative activation stimuli, we sought to determine how polarizing stimuli affect neurotoxic or neuroprotective activity. The critical role played by classically activated astrocytes in neuronal cell death was demonstrated previously (49, 50). To determine how classical or alternative activation of astrocytes influences neuronal viability, we used ACM (Fig. 3A) and astrocyte–neuron coculture (Fig. 3B). To examine the effects of soluble factors secreted by classically or alternatively activated astrocytes on neuronal survival/death, we collected ACM after stimulating cultured astrocytes with LPS/IFN-γ, IL-4, or IL-10 and added these to cortical neuron cultures. Neuronal cell viabilities were assessed using an MTT assay. Compared with control ACM-treated neurons, LPS/IFN-γ ACM reduced neuronal viability. In contrast, although IL-4 or IL-10 ACM alone did not affect neuronal viability, they did attenuate neuronal cell death induced by excitotoxicity (glutamate) or oxidative stress (H_2O_2). LPS/IFN-γ ACM enhanced glutamate- or H_2O_2-induced neuronal cell death. The concentrations of glutamate and H_2O_2 that reduced cortical neuron viability by ∼50% compared with untreated neurons were used in this study. Our results indicate that classically activated astrocytes are neurotoxic, but that alternatively activated astrocytes protect neurons against excitotoxic or oxidative injuries (Fig. 3A). Because TNF-α has been linked to neuronal death, we determined the contribution of TNF-α to neurotoxicity of LPS/IFN-γ–stimulated ACM. Neutralization of TNF-α in the LPS/IFN-γ–stimulated ACM using anti-TNF-α Ab reduced the neurotoxicity, indicating an important role for TNF-α in the

neurotoxicity of classically activated astrocytes (neuronal viability after treatment with LPS/IFN-γ–stimulated ACM, 81.1 ± 1.6%; neuronal viability after treatment with LPS/IFN-γ–stimulated ACM plus anti–TNF-α Ab, 91.6 ± 2.4%; $p < 0.05$). Based on the TNF-α concentration in the astrocyte culture media as determined by ELISA (Fig. 2A), 3-fold molar concentration of anti-TNF-α Ab (400 ng/ml) was used for the neutralization experiment. To examine the neurotoxic and neuroprotective effects of phenotypically polarized astrocytes further, coculture of astrocytes and neurons was performed using culture inserts (Fig. 3B). LPS/IFN-γ–stimulated astrocytes significantly reduced neuronal cell viability in coculture for 24 h, and IL-4 or IL-10 stimulation of astrocytes did not significantly affect the viability of cocultured neurons. The coculture of LPS/IFN-γ−stimulated astrocytes and neurons for 48–72 h further enhanced neuronal cell death (data not shown). Taken together, our results indicate that classically or alternatively activated astrocytes exert neurotoxic or neuroprotective activities, respectively. Thus, functionally polarized astrocytes seem to display distinct gene-expression patterns, as well as different effector functions.

Functional polarization of astrocytes in vivo

To confirm the classical or alternative activation of astrocytes in vivo, the expression of phenotypic markers was assessed after injecting LPS or IL-4 i.c.v. into mouse brain (Table II). After injecting saline, LPS, or IL-4, adult astrocytes were isolated, and the expression of classical and alternative activation markers was analyzed. LPS or IL-4 injection induced the expression of genes associated with classical or alternative activation in isolated astrocytes, respectively, suggesting the induction of functionally polarized phenotypes of astrocytes in vivo. Phenotypic polarization of astrocytes was further investigated in vivo using a mouse neuroinflammation model, which is dominated by the proinflammatory classical activation of astrocytes. We asked whether alternative
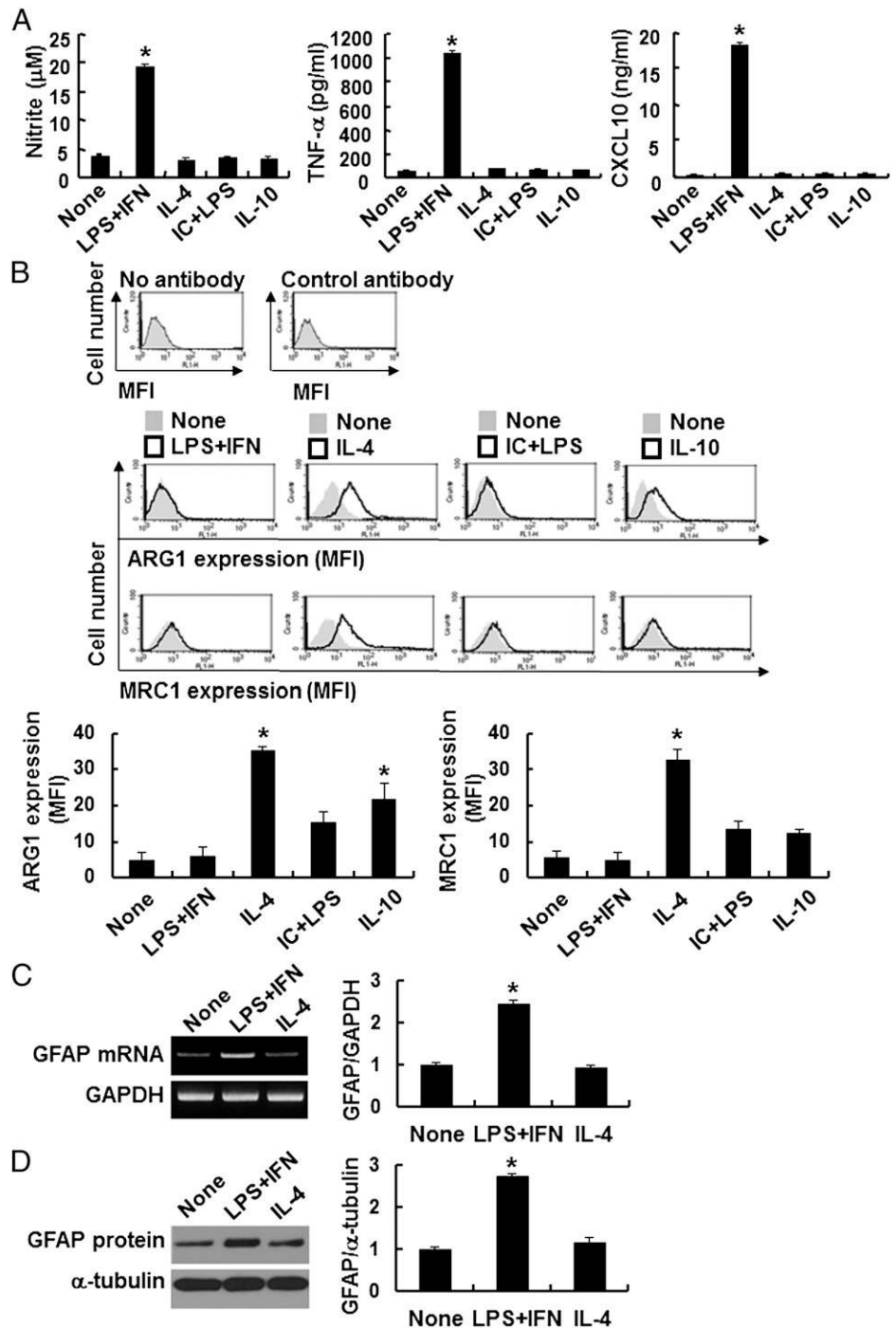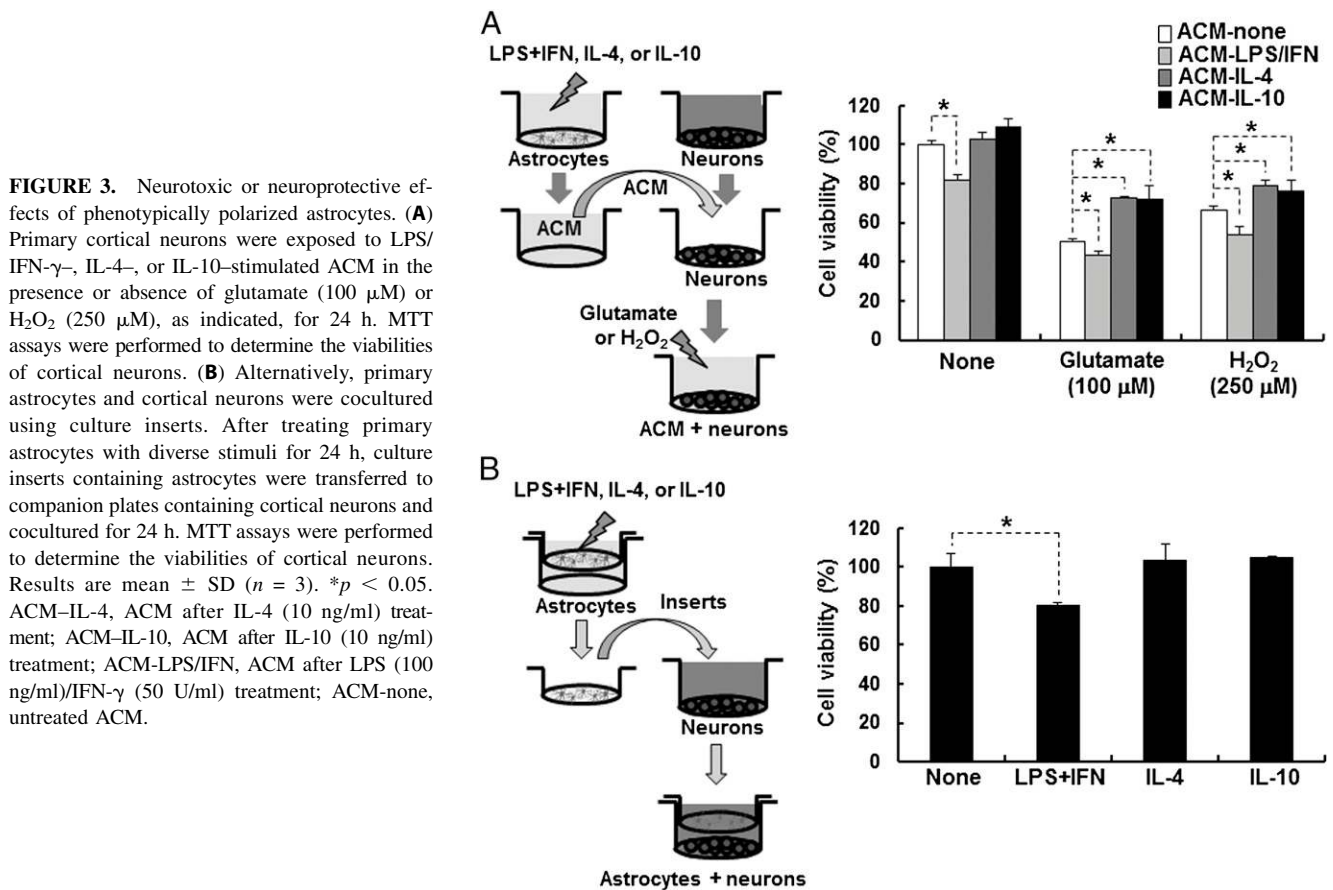
FIGURE 2. Assessment of NO production, TNF-α/CXCL10 secretion, expression of ARG1/MRC1 proteins, and GFAP levels following exposure to either classical or alternative activation stimuli. Primary astrocyte cultures were treated with LPS (100 ng/ml) plus IFN-γ (50 U/ml), IL-4 (10 ng/ml), IC (OVA [75 μg/ml] plus OVA Ab [150 μg/ml]) plus LPS (100 ng/ml), or IL-10 (10 ng/ml) for 24 h. (**A**) Concentrations of nitrite, TNF-α protein, and CXCL10 protein in culture media were measured using Griess reagent or specific ELISA. (**B**) ARG1 and MRC1 protein expression was detected by flow cytometry using Abs specific for ARG1 or MRC1. Mean fluorescence intensity (MFI) values are also shown. Negative control is the measurement without specific Ab or with a control Ab. GFAP mRNA or protein levels were evaluated by RT-PCR (**C**) or Western blotting (**D**), respectively. *Gapdh* or α-tubulin was used as an internal control. Results are mean ± SD ($n = 3$). *$p < 0.05$, versus untreated control.

activation would reduce proinflammatory gene expression in this neuroinflammation model. A peripheral injection of LPS (5 mg/kg) was used to induce neuroinflammation in mice, as previously described (41). A preinjection of IL-4 (i.c.v.) was given to induce the alternative activation of astrocytes directly. Twelve hours after the i.c.v. injection of saline or IL-4, LPS was injected i.p.; mice were sacrificed 24 h later, and astrocytes were isolated for gene-expression analysis. Compared with saline preinjection, IL-4 pre-injection into brain reduced the expression of proinflammatory genes associated with the classical activation of astrocytes (*Il-1β*, *Inos*, *Tnf-α*, and *Cxcl10*) in the LPS-induced neuroinflammation model (Fig. 4A). LPS-induced neuroinflammation and the effect of IL-4 were also determined by histological analyses (Supplemental Fig. 2). Injection (i.p.) of LPS induced glial activation and

inducible NO synthase (iNOS) expression, which was attenuated by IL-4 preinjection (i.c.v.). In a previous study, preinjection of IL-4 reduced LPS-induced sickness behavior (51), which suggests that animal behavior may reflect the functional polarization of astrocytes. Open-field testing showed that the locomotive activities of LPS-injected mice were lower than those of saline-injected controls (Fig. 4B). IL-4 preinjection ameliorated LPS-induced locomotive impairment (i.e., IL-4 preinjection partly abolished LPS-induced reduction of total distance traveled and movement speed). These results support that the functional and phenotypic dichotomy of activated astrocytes (classical or alternative activation) exist in vivo. To exclude the potential contributions of microglia/macrophages to behavioral changes, clodronate was injected i.p. and i.c.v. to eliminate microglia/macrophage populations in the

FIGURE 3. Neurotoxic or neuroprotective effects of phenotypically polarized astrocytes. (**A**) Primary cortical neurons were exposed to LPS/IFN-γ–, IL-4–, or IL-10–stimulated ACM in the presence or absence of glutamate (100 μM) or H_2O_2 (250 μM), as indicated, for 24 h. MTT assays were performed to determine the viabilities of cortical neurons. (**B**) Alternatively, primary astrocytes and cortical neurons were cocultured using culture inserts. After treating primary astrocytes with diverse stimuli for 24 h, culture inserts containing astrocytes were transferred to companion plates containing cortical neurons and cocultured for 24 h. MTT assays were performed to determine the viabilities of cortical neurons. Results are mean ± SD ($n = 3$). *$p < 0.05$. ACM–IL-4, ACM after IL-4 (10 ng/ml) treatment; ACM–IL-10, ACM after IL-10 (10 ng/ml) treatment; ACM-LPS/IFN, ACM after LPS (100 ng/ml)/IFN-γ (50 U/ml) treatment; ACM-none, untreated ACM.

periphery, as well as in the CNS (Fig. 5A). Reduction of microglia and macrophage counts in brain and liver was confirmed by Iba-1 immunohistochemistry (Supplemental Fig. 3). In clodronate-injected mice, LPS induced classical astrocyte activation, which was attenuated by IL-4 pretreatment (Fig. 5B). The LPS-induced impairments in locomotion and hippocampus-dependent memory were also alleviated by IL-4 preinjection of clodronate-treated mice in the open-field test and the object-recognition task, respectively (Fig. 5C, 5D). The tail-suspension test was performed to determine the effect of IL-4 on LPS-induced depression-like

behavior, and LPS-induced immobility was significantly diminished by IL-4 preinjection (Fig. 5E). The elimination of microglia/macrophages did not affect astrocyte polarization or related animal behavior.

The association between LCN2 expression and the classical activation of astrocytes in culture

LCN2 is a member of the lipocalin family that has the conserved β-barrel structure. LCN2 acts as a potent bacteriostatic agent by sequestering iron. In addition to its role in iron delivery, LCN2

Table II. Astrocyte polarization in vivo and the role of LCN2 in classical activation

	LPS		IL-4	
	Lcn2 WT	*Lcn2* KO	*Lcn2* WT	*Lcn2* KO
Classical activation-related genes				
Il-1β	5.59 ± 0.98*	1.03 ± 0.11**	1.08 ± 0.66	1.39 ± 0.48
Inos	10.41 ± 0.84*	1.59 ± 0.26**	1.56 ± 0.22	0.96 ± 0.10
Tnf-α	16.44 ± 0.95*	1.54 ± 0.43**	0.95 ± 0.56	1.23 ± 0.31
Cxcl10	12.65 ± 0.83*	1.14 ± 0.11**	0.93 ± 0.12	1.24 ± 0.11
Il-12	1.08 ± 0.31	1.17 ± 0.18	1.17 ± 0.42	1.45 ± 0.24
Il-23	1.43 ± 0.48	0.89 ± 0.09	1.14 ± 0.23	1.01 ± 0.13
Alternative activation-related genes				
Il-10	1.25 ± 0.20	1.20 ± 0.18	3.88 ± 1.19*	4.04 ± 0.48*
Arg1	1.36 ± 0.15	1.33 ± 0.21	2.36 ± 0.51*	2.37 ± 0.36*
Mrc1	1.32 ± 0.46	1.07 ± 0.20	4.71 ± 0.24*	3.96 ± 1.16*
Il-1ra	1.10 ± 0.17	1.06 ± 0.11	3.34 ± 0.25*	3.48 ± 0.36*
Fizz1	1.36 ± 0.43	1.41 ± 0.50	4.89 ± 0.16*	5.33 ± 0.74*
Ym1	1.01 ± 0.05	1.50 ± 0.34	3.21 ± 0.16*	3.44 ± 0.08*

Lcn2 WT or KO mice were administered an i.c.v. injection of saline ($n = 4$), LPS (5 μg; $n = 5$), or IL-4 (100 ng; $n = 5$). After 24 h, adult astrocytes were isolated from animal brains to determine the mRNA levels of proinflammatory or anti-inflammatory genes by real-time RT-PCR. *Gapdh* was used as an internal control.

Data are mean (± SD) fold change of specific mRNA expression versus saline-treated controls.

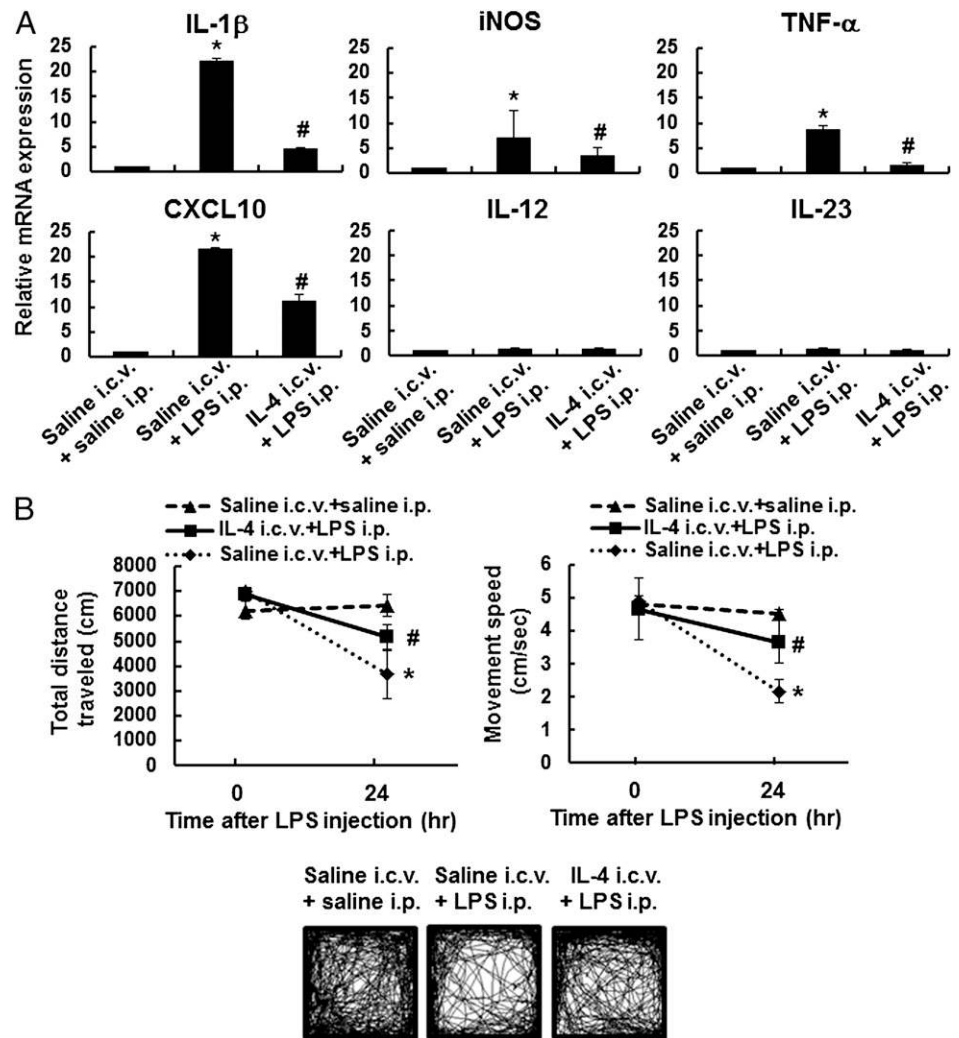*$p < 0.05$, versus saline-treated controls; **$p < 0.05$, Lcn2 WT versus KO mice.

FIGURE 4. Inhibition of astrocyte classical activation by IL-4 in a neuro-inflammation model. IL-4 (100 ng) was injected (i.c.v.) into WT mice 12 h prior to LPS (5 mg/kg, i.p.). At 24 h after the LPS injection, adult astrocytes were isolated from animal brains for RNA analysis (**A**), or mice were subjected to the open-field test (see *Materials and Methods* for details) (**B**). The mRNA levels of classical activation-related genes were determined by real-time RT-PCR, and *Gapdh* was used as an internal control (A). Total distance traveled in 30 min and speed were measured using the open-field test (B). Black lines represent the paths of animals in the arena, as determined using a video-tracking system (*lower panels*). The results shown are mean ± SD ($n = 5$ for each experimental group). *$p < 0.05$, versus saline-injected (i.c.v. and i.p.) controls, #$p < 0.05$, versus LPS-injected (i.p.) mice.

takes part in angiogenesis, febrile response, insulin resistance, and inflammation as an acute-phase protein. LCN2 regulates diverse cellular processes, including cell death/survival, cell migration, and cell differentiation. In a previous study, proinflammatory stimuli induced the expression of LCN2 in astrocytes, which acted as an autocrine mediator of reactive astrocytosis (26); thus, we set out to determine how the expression of LCN2 is regulated by classical or alternative activation stimuli in astrocytes. The gene expression and secretion of LCN2, as determined by real-time RT-PCR and ELISA, respectively, were strongly enhanced by LPS/IFN-γ in primary astrocyte cultures (Fig. 6A, 6B). However, no alternative activation stimuli (IL-4, IC+LPS, or IL-10) significantly affected LCN2 expression, indicating that LCN2 expression is elevated in classically activated, but not in alternatively activated, astrocytes. We next sought to determine whether LCN2 secreted by classically activated astrocytes influences the phenotypic polarization of cultured astrocytes (Fig. 6C). LCN2-treated astrocytes expressed phenotypic markers representative of classical activation (*Il-1β*, *Inos*, *Tnf-α*, and *Cxcl10*), but not those of alternative activation (*Il-10*, *Arg1*, *Mrc1*, *Il-1ra*, *Fizz1*, and *Ym1*), at high levels. Proinflammatory *Il-12* and *Il-23* levels were not induced by LCN2, which was consistent with the effect of LPS/IFN-γ. rGST protein, which was purified during the process of LCN2 preparation (26), was used as a control for LCN2 (Fig. 6C). LCN2 protein purified from mammalian cells (M-LCN2) showed similar effects on the proinflammatory gene expression (Fig. 6D). The possibility of

endotoxin contamination of recombinant LCN2 was ruled out by multiple means: treatment of LCN2 preparation with polymyxin B, neutralization of LCN2 activity using anti-LCN2 Ab, and use of denatured LCN2 protein. LCN2 was reported to induce NO production in astrocytes (26), and, in the current study, this LCN2-induced NO production was not abolished by polymyxin B treatment (Supplemental Fig. 4). LCN2-induced NO production was significantly reduced by LCN2 Ab neutralization. Denatured LCN2 preparation had no significant effect on NO production (Supplemental Fig. 4). These results indicate that the effects of LCN2 observed in this study are not due to endotoxin contamination. Taken together, our results support the notion that LCN2 promotes the classical activation of astrocytes in an autocrine manner. The expression of astrocytic LCN2 receptors (*24p3R* and *Megalin*) (13, 52) was not significantly influenced by either classical or alternative activation (Fig. 6E).

LCN2 inhibition of alternative activation pathway in cultured astrocytes

Having found that LCN2 promotes the classical activation of astrocytes, we examined whether LCN2 regulates alternative activation signaling in astrocytes. Because IL-4–STAT6 is a canonical pathway of alternative activation (53, 54), we investigated the effect of LCN2 on this pathway. The phosphorylation status of STAT6 at tyrosine residue 641 was assessed by Western blot analysis to determine whether LCN2 affects IL-4–induced STAT6

FIGURE 5. Functional polarization of astrocytes in the absence of microglia/macrophages. (**A**) Mice were injected with liposome-encapsulated clodronate (i.p. and i.c.v.) to remove macrophages and microglia. At 72 h after clodronate injection, IL-4 (100 ng, i.c.v.) was injected, followed 12 h later by an LPS injection (5 mg/kg, i.p.). At 24 h after the LPS injection, adult astrocytes were isolated from animal brains for RNA analysis (**B**), or mice were subjected to the open-field test (**C**), object-recognition task (**D**), or the tail-suspension test (**E**). (B) The mRNA levels of classical activation-related genes were determined by real-time RT-PCR, and *Gapdh* was used as an internal control. (C) Total distances traveled in 30 min were measured using the open-field test. (D) Hippocampus-dependent cognitive deficits were detected using the object-recognition task. Exploration times are expressed as DIs, defined as $(N - F)/(N + F)$, where N is the time spent at the novel object, and F is the time spent at the familiar object. (E) Immobility times were determined using the tail-suspension test, as described in *Materials and Methods*. Results are mean ± SD ($n = 3$). *$p < 0.05$ versus saline-injected (i.c.v. and i.p.) controls, #$p < 0.05$, versus LPS-injected (i.p.) mice.
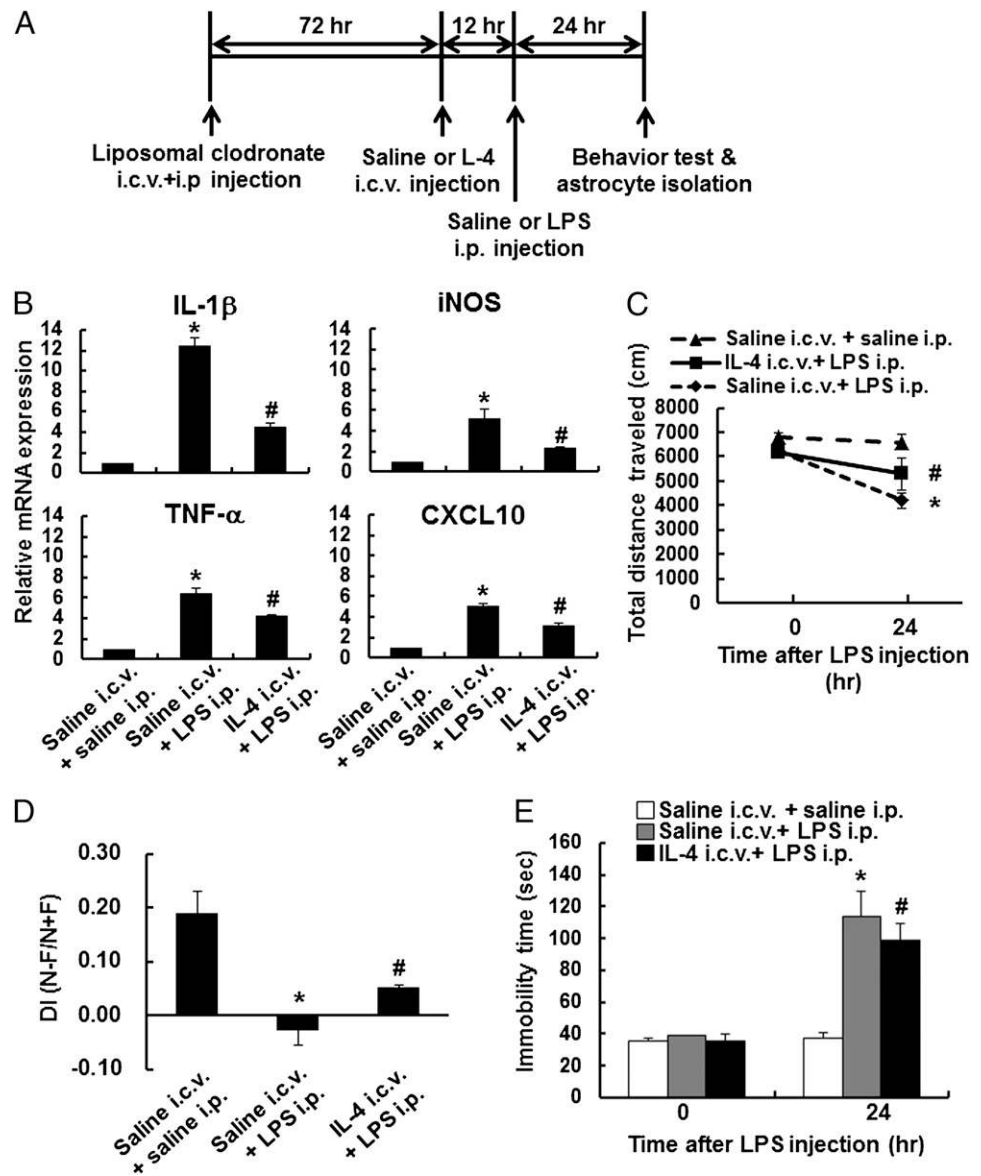
signaling associated with the alternative activation of astrocytes. The phosphorylation of STAT6 was observed at 30 min after IL-4 stimulation, and LCN2 significantly inhibited IL-4–induced STAT6 phosphorylation in primary astrocytes (Fig. 7A). LCN2 also inhibited the expression of genes (*Il-10*, *Arg1*, *Mrc1*, *Il-1ra*, *Fizz1*, and *Ym1*) downstream of IL-4–STAT6 (Fig. 7B). Leflunomide, a pharmacological inhibitor of JAK3/STAT6, was used as a control (Fig. 7B). Flow cytometric analysis indicated that IL-4–induced expression of ARG1 and MRC1 proteins was similarly decreased by LCN2 (Fig. 7C).

Pivotal role of LCN2 in the classical activation of astrocytes

To confirm the role of LCN2 in the classical activation of astrocytes, we compared the gene-expression profiles of astrocytes isolated from *Lcn2* WT and KO mice by comparing classical and alternative activation–related gene expression in primary astrocytes isolated from WT and KO mice exposed to LPS/IFN-γ, IL-4, IC+LPS, or IL-10. In *Lcn2*-deficient astrocytes, the LPS/IFN-γ induction of genes associated with classical activation (*Il-1β*, *Inos*, *Tnf-α*, and *Cxcl10*) was completely abolished (Fig. 8A). Furthermore, the induction of genes associated with alternative activation (*Il-10*, *Arg1*, *Mrc1*, *Il-1ra*, *Fizz1*, and *Ym1*) in response to

IL-4 or IL-10 was not significantly affected (or slightly increased) by *Lcn2* deficiency (Fig. 8B). We next investigated the in vivo role of LCN2 in the functional polarization of astrocytes in the brains of WT or *Lcn2* KO mice following an i.c.v. injection of LPS or IL-4, which directly induced the classical or alternative activation of astrocytes, respectively (Table II). Animals were administered an i.c.v. injection of saline, LPS, or IL-4; mice were sacrificed 24 h later, and adult astrocytes were isolated from whole brains to evaluate the expression of classical or alternative activation-related genes. In WT mice, LPS or IL-4 administration induced the genes associated with classical or alternative activation, respectively, in astrocytes (Table II). However, in *Lcn2*-deficient mice, the LPS induction of classical activation genes was completely abrogated, whereas the induction of alternative activation genes by IL-4 was not significantly influenced, which further supported the pivotal role played by LCN2 in the classical activation of astrocytes. LCN2 induction and its role in classically activated astrocytes were investigated further by immunohistochemical analysis of brain sections from *Lcn2* WT and KO mice after an i.c.v. injection of LPS or IL-4 (Figs. 9, 10). In LPS-injected WT mice, the expression of GFAP, LCN2, and iNOS was induced in the cortex, and GFAP expression was partly colocalized with LCN2
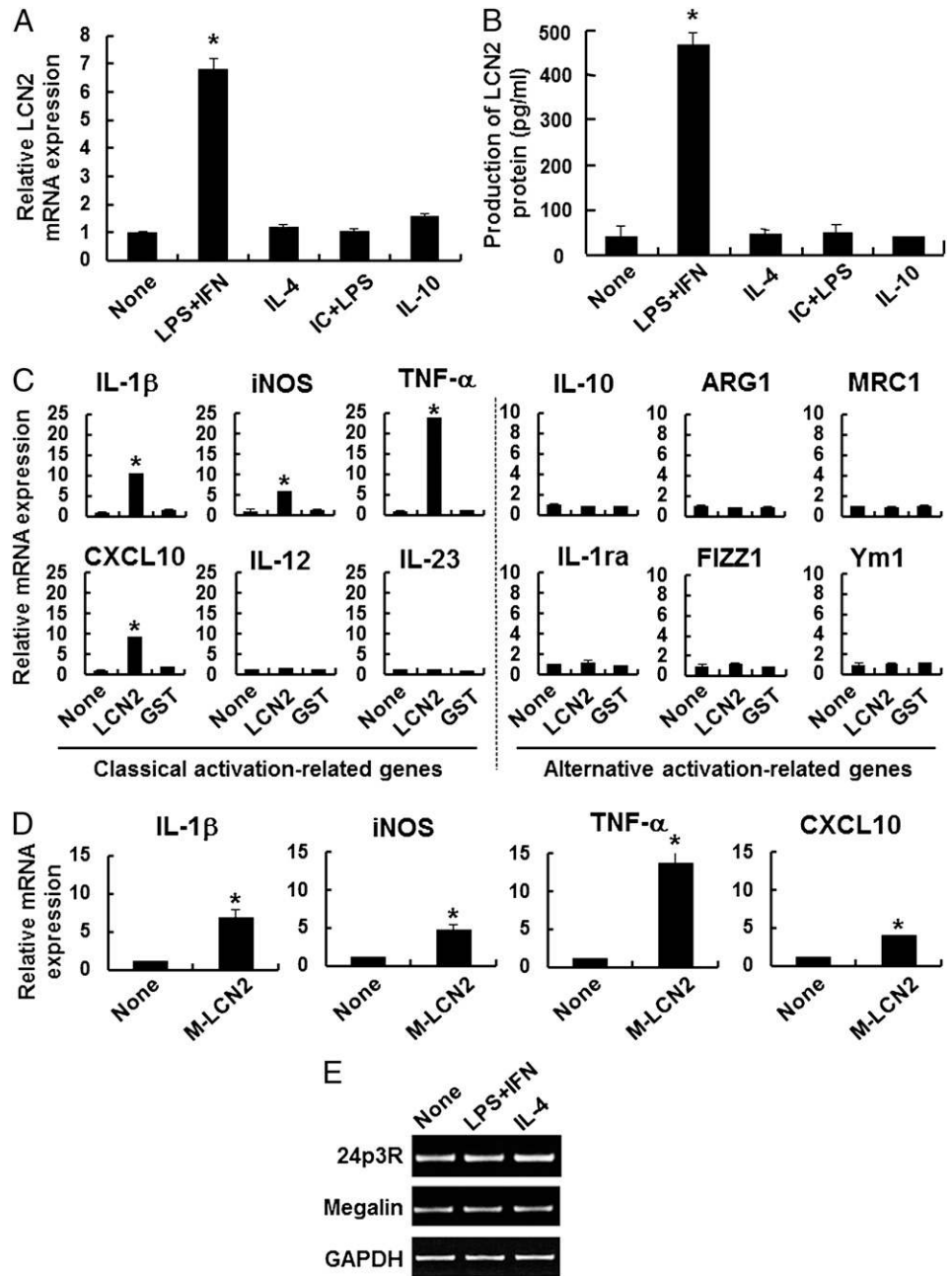
FIGURE 6. Association between classical astrocyte activation and LCN2. The expression of LCN2 mRNA and protein were assessed by real-time RT-PCR (**A**) or ELISA (**B**) after primary astrocytes were treated with classical or alternative activation stimuli for 8–24 h (8 h for real-time RT-PCR; 24 h for ELISA). Primary astrocyte cultures were treated with recombinant LCN2 protein (10 μg/ml), GST protein (10 μg/ml) (**C**), or LCN2 protein prepared from mammalian cells (M-LCN2) (10 μg/ml) (**D**) for 8 h, and the mRNA levels of different polarization markers were measured by real-time RT-PCR. (**E**) Levels of LCN2 receptor (*24p3R* and *Megalin*) mRNA in the primary astrocytes were compared by traditional RT-PCR after LPS/IFN-γ or IL-4 treatment (8 h). The results are mean ± SD ($n = 3$). *$p < 0.05$, versus untreated controls.

and iNOS expression at 24 h after LPS injection, demonstrating the induction of LCN2 and the classical activation of GFAP[+] astrocytes (Fig. 9). We previously showed that LPS or IL-4 injection induced microglial polarization in vivo (47). Unlike astrocytes, microglial expression of iNOS was observed at 48 h, but not at 24 h, after LPS injection (47). Thus, astrocytes and microglia seem to show distinct time kinetics with respect to the expression of iNOS and other proinflammatory mediators in vivo. The LPS-induced phenotypic changes of astrocytes were markedly attenuated in *Lcn2* KO mice; numbers of GFAP-expressing and iNOS-expressing cells were reduced by *Lcn2* deficiency. A similar increase in GFAP expression was observed in hippocampus after LPS injection, whereas a decrease was observed in *Lcn2* KO mice (Fig. 9). Furthermore, DAPI staining showed that LPS injection induced hippocampal injury and that this was attenuated by *Lcn2* deficiency. Because LPS injection induced the expression of iNOS (a representative classical activation marker) in the cortex, we next sought to determine whether the injection of IL-4 induces the expression of alternative activation markers in the cortex. As expected, the alternative activation marker ARG1 in astrocytes was induced 48 h after IL-4 injection (Fig. 10). In microglia, IL-4 injection induced ARG1 expression at 24 h (47). However, in astrocytes, ARG1 expression was detected at 48 h after IL-4 injection. The induction of ARG1 in cortical astrocytes was not significantly influenced by *Lcn2* deficiency (Fig. 10). Furthermore, numbers of GFAP^{+} cells were not significantly changed by *Lcn2* deficiency. These histological findings confirm that the functional polarization of astrocytes can be induced in experimental animals, as well as that LCN2 plays a central role in the classical activation of astrocytes.

The additional role of LCN2 in the regulation of the polarized phenotypes of astrocytes

We previously demonstrated that the length and number of cellular processes were increased in classically activated astrocytes.
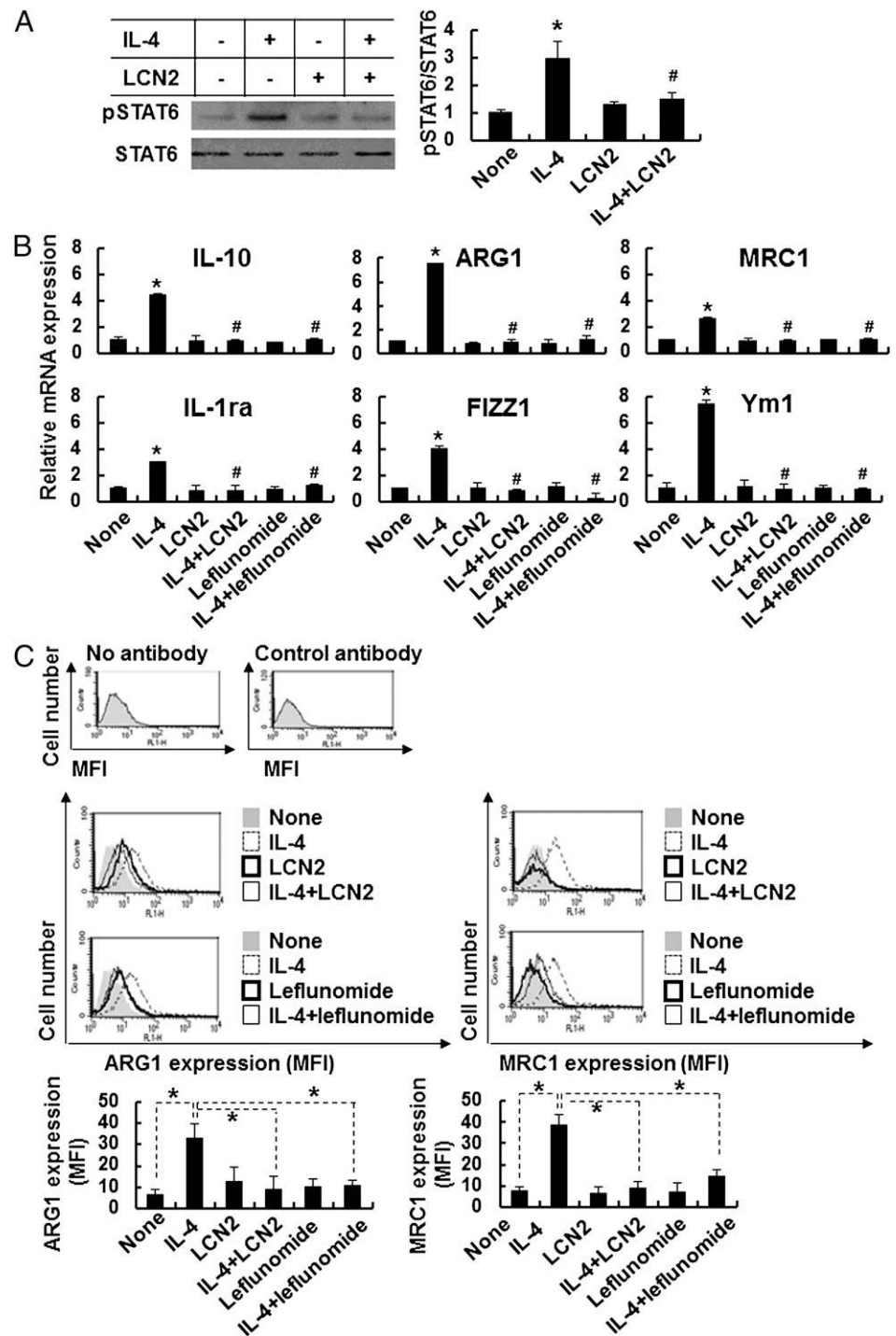
FIGURE 7. LCN2 inhibition of IL-4–induced STAT6 phosphorylation and its downstream gene expressions in astrocytes. Primary astrocyte cultures were treated with IL-4 (10 ng/ml), recombinant LCN2 protein (10 μg/ml), or leflunomide (10 μM) (30 min for Western blot analysis; 8 h for real-time RT-PCR; and 24 h for flow cytometric analysis). (**A**) Levels of phosphorylated STAT6 (pSTAT6 at Tyr[641]) and total STAT6 protein were evaluated by Western blotting. (**B**) The mRNA levels of alternative activation-related genes were quantified by real-time RT-PCR. *Gapdh* was used as an internal control. (**C**) ARG1 and MRC1 protein expression was evaluated by flow cytometry. Mean fluorescence intensity (MFI) values are also shown. Negative control is the measurement without specific Ab or with a control Ab. Results are mean ± SD ($n = 3$). *$p < 0.05$, versus untreated controls or between the treatments indicated, #$p < 0.05$, versus IL-4 alone.

Furthermore, in the current study, ACM transfers and astrocyte–neuron cocultures revealed that classically activated astrocytes are neurotoxic (Fig. 3). In addition, alternatively activated astrocytes showed distinct phenotypes with neuroprotective activity. To determine the role played by LCN2 in the regulation of these functional phenotypes, the phenotypes of astrocytes derived from WT and *Lcn2* KO mice were compared. In *Lcn2*-deficient astrocytes in culture, the LPS/IFN-γ–induced increase in GFAP expression was diminished (Fig. 11A). Furthermore, the neurotoxicity of classically activated astrocytes was reduced by *Lcn2* deficiency (Fig. 11B, 11C). The neurotoxic effects exerted by the transfer of ACM following LPS/IFN-γ stimulation (Fig. 11B) and by coculture of

LPS/IFN-γ–stimulated astrocytes with cortical neurons (Fig. 11C) were attenuated by *Lcn2* deficiency in astrocytes. The effects of IL-4 were unchanged by the presence or absence of *Lcn2* in astrocytes.

Discussion

Astrocytes support neuronal functions in many ways (e.g., by providing guidance cues and neurotrophic factors); thus, impaired astrocytic function has major consequences on neuronal function. Activated astrocytes can express diverse cytokines, chemokines, and their receptors and, thus, have pivotal roles in the neuroinflammatory process. Furthermore, the changes caused by astrocyte
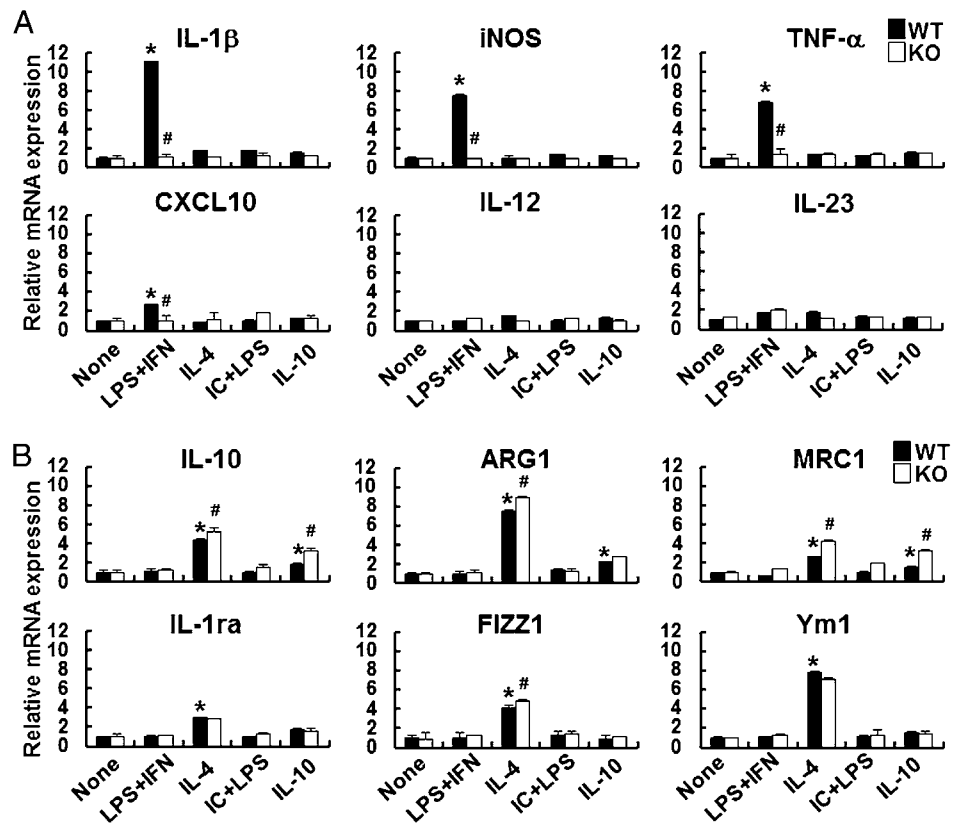
FIGURE 8. Essential role of LCN2 in the classical, but not in the alternative, activation of cultured astrocytes. Primary astrocyte cultures prepared from *Lcn2* WT (n = 3) or KO (n = 3) mice were treated with LPS (100 ng/ml) plus IFN-γ (50 U/ml), IL-4 (10 ng/ml), ICs (OVA [75 μg/ml] plus OVA Ab [150 μg/ml]) plus LPS (100 ng/ml), or IL-10 (10 ng/ml) for 8 h, and the mRNA levels of classical activation-related genes (**A**) or alternative activation-related genes (**B**) were compared by real-time RT-PCR. *Gapdh* was used as an internal control. Results are mean ± SD (n = 3). *$p < 0.05$, versus untreated controls, #$p < 0.05$, *Lcn2* WT versus KO mice.

activation can beneficially or deleteriously impact neuronal function and survival (55). Functional and structural heterogeneity of astrocytes was reported (56, 57). Astrocytes exhibited functional heterogeneity with respect to membrane conductance (58, 59), expression of transmitter receptors (60), extent of gap junction coupling (61), glutamate transporter expression (62), and Ca^{2+} signaling (63). Diverse astrocyte morphologies across various regions of the CNS also were observed, hinting at an extensive reservoir of astrocyte molecular heterogeneity (64). Comparison of gene signature of astrocytes supported astrocyte heterogeneity (65, 66). However, the existence of functionally polarized phenotypes of astrocytes under immune and inflammatory condition has not been clearly established. Moreover, little is known about the regulatory mechanism underlying the phenotypic polarization of astrocyte activation. In this study, we demonstrate that astrocytes activated under neuroinflammatory conditions show classical or alternative activation and that LCN2 promotes their classical inflammatory activation.

It is well established that the expression of proinflammatory genes in astrocytes is increased by LPS/IFN-γ, and it was demonstrated that robust increases in GFAP expression and process extension are induced by LPS/IFN-γ (67). In agreement with these previous findings, LPS/IFN-γ–activated astrocytes showed increased expression of classical activation-related genes and GFAP. NO production and TNF-α and CXCL10 protein secretions were also increased in classically activated astrocytes. Moreover, LPS/IFN-γ–activated astrocytes were toxic to neurons in this study, which is consistent with previous reports in which LPS/IFN-γ–activated astrocytes killed neurons by inducing inflammatory mediators like IL-1β and TNF-α in vitro (68, 69). In contrast to the classical activation condition, alternative activation stimuli, such as IL-4 and IL-10, induced the expression of distinct phenotypic markers in astrocytes. The opposing roles of LPS/IFN-γ

and IL-4/IL-10 in the functional regulation of astrocytic phenotypes has been documented extensively. For instance, LPS led to a significant increase in GFAP expression in glia, but IL-4 had no effect (70), and although LPS and proinflammatory cytokines reduced levels of brain-derived neurotrophic factor in astrocytes, IL-4 increased them (71). Moreover, glucose use was increased in classically activated astrocytes, but it was attenuated by IL-10 (72). Furthermore, under neuroinflammatory disease conditions, IL-4 and IL-10 downregulated the expression of glial iNOS, TNF-α, and ICAM-1 (73, 74).

In a model of experimental autoimmune encephalomyelitis, expression of the alternative activation marker ARG1 protein was increased in infiltrating astrocytes during the remitting phase of the disease, which suggests that alternatively activated astrocytes play an anti-inflammatory or neuroprotective role (75). IL-4 was reported to induce the release of neuroprotectants from astrocytes exposed to oxidative stress and, thus, to limit proinflammatory neurotoxic responses (76). In the current study, IL-4– and IL-10–activated astrocytes also mediated neuroprotective effects against excitotoxic or oxidative insults. The neuroprotective factors released by IL-4– or IL-10–activated astrocytes have not been precisely characterized. Nevertheless, STAT6 is a key component of the intracellular pathway downstream of IL-4 signaling, and the IL-4–STAT6 axis is likely to orchestrate various phenotypes of alternatively activated astrocytes, including the expression of specific phenotypic markers and neuroprotective molecules. A recent study found that phosphorylation of STAT6 was induced by IL-4 in astrocytes (77), which concurs with our finding that STAT6 was phosphorylated in IL-4–activated astrocytes. In addition, we present evidence that LCN2 targets IL-4–STAT6 signaling to inhibit the alternative activation of astrocytes (see later discussion). However, LCN2 inhibition of the IL-4–STAT6 pathway is not highly unexpected because of the known cross-inhibitory ability of NF-κB
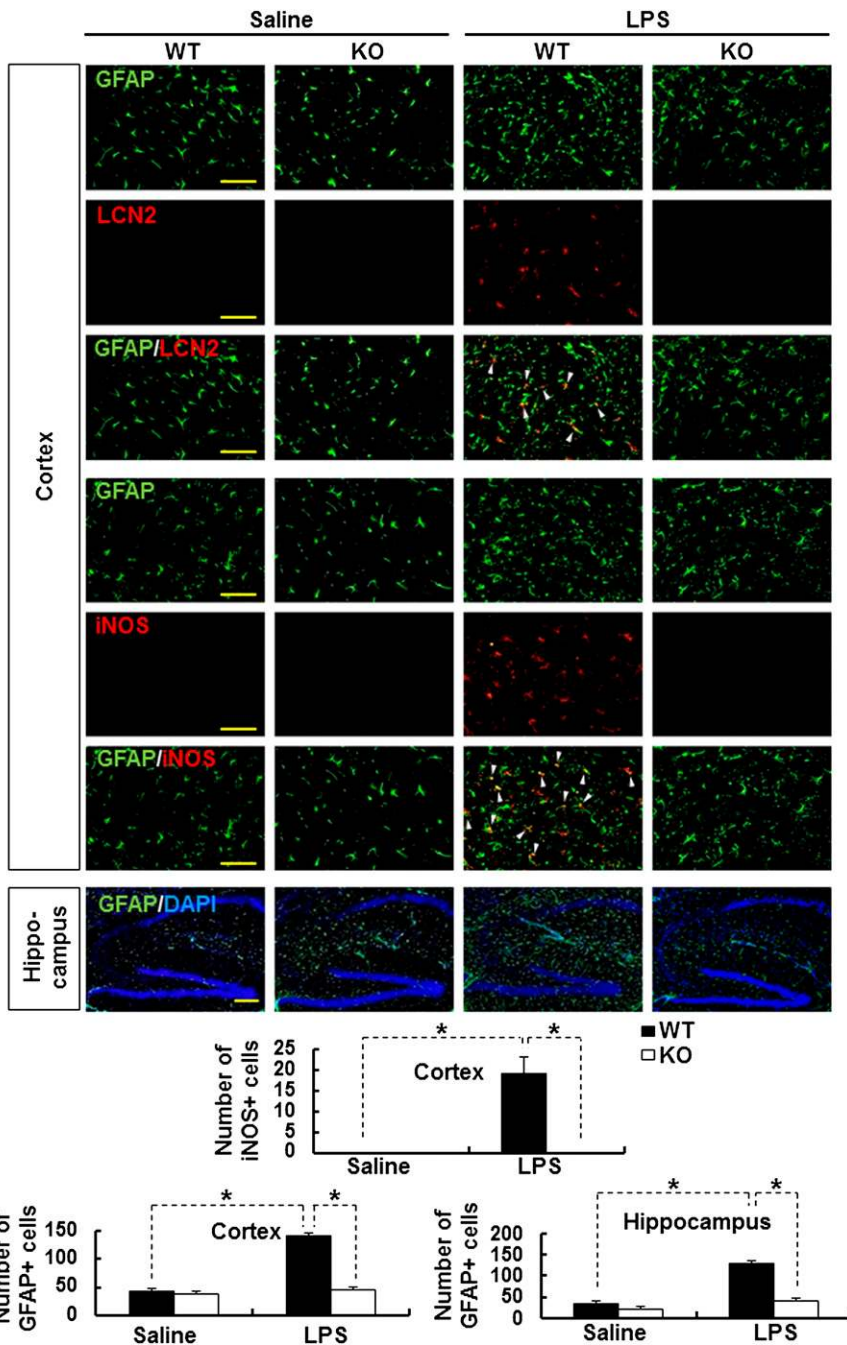
FIGURE 9. Immunohistochemical analysis of LCN2 expression and astrocyte classical activation. Brain cortex or hippocampus sections were stained with Abs against GFAP (green), LCN2 or iNOS (red), or DAPI (nuclei; blue) 24 h after injecting *Lcn2* WT (*n* = 5) or KO mice (*n* = 5) with saline or LPS (5 μg, i.c.v.). LCN2 and iNOS expression increased significantly in cortices 24 h after LPS administration and colocalized with GFAP (colocalization is indicated by the arrowheads), showing that astrocytes expressed LCN2 and iNOS following LPS exposure. Scale bars, 100 μm (cortex), 200 μm (hippocampus). Numbers of cells expressing iNOS or GFAP were counted and compared between *Lcn2* WT and KO mice. Results are mean ± SD (*n* = 5). *$p < 0.05$.

and STAT6. IL-4 appears to inhibit the classical activation of astrocytes in vivo. In our neuroinflammation model, pretreatment with IL-4 abolished LPS-induced gene expression and improved motor impairment in vivo, which is in line with previous findings that IL-4 attenuated LPS-induced proinflammatory cytokines and sickness behaviors (51). Therefore, classical or alternative activation stimuli seem to induce respective phenotypic changes and inhibit opposite phenotypes in astrocytes. Recently, IRF-3 was suggested to be a regulator of the astrocyte activation phenotype. It suppressed proinflammatory astrocytic activation by regulating immunomodulatory microRNA expression (78); however, the effect of LCN2 on IRF-3 has yet to be examined.

LCN2 has been implicated in several inflammatory pathologies of the CNS (23–25, 27–30, 32, 79–81). In mouse models of ce-

rebral ischemia and neuroinflammation, LCN2 was found to be prominently induced in astrocytes (81). In a previous study, we found that LCN2 promotes morphological changes and cell migration of astrocytes in an autocrine manner (26, 37), and increasing evidence now suggests that LCN2 is a key regulator of brain inflammation. In the current study, LCN2 was induced by classically, but not by alternatively, activated astrocytes, and LCN2 promoted the classical activation of astrocytes but suppressed the alternative activation phenotype by inhibiting STAT6 phosphorylation, a canonical pathway of alternative activation. Furthermore, LCN2 caused the expression of classical activation-related genes and GFAP in astrocytes. The expression of phenotypic markers of classical activation and GFAP was reduced in astrocytes derived from *Lcn2* KO mice, and *Lcn2* deficiency in astrocytes attenuated the neurotoxic effects of LPS/IFN-γ in astrocytes. The LCN2 receptors (*24p3R*

FIGURE 10. Identification of astrocyte alternative activation in brain tissues by immunohistochemistry. GFAP (green) and ARG1 (red) expression was assessed by immunohistochemistry in brain cortex 48 h after injecting *Lcn2* WT mice (*n* = 5) or KO mice (*n* = 5) with saline or IL-4 (100 ng, i.c.v.). Scale bar, 100 μm. Arrowheads indicate the colocalization of GFAP and ARG1. Numbers of cells expressing GFAP or ARG1 were counted and compared between *Lcn2* WT and KO mice. Results are mean ± SD (*n* = 5). *$p < 0.05$.
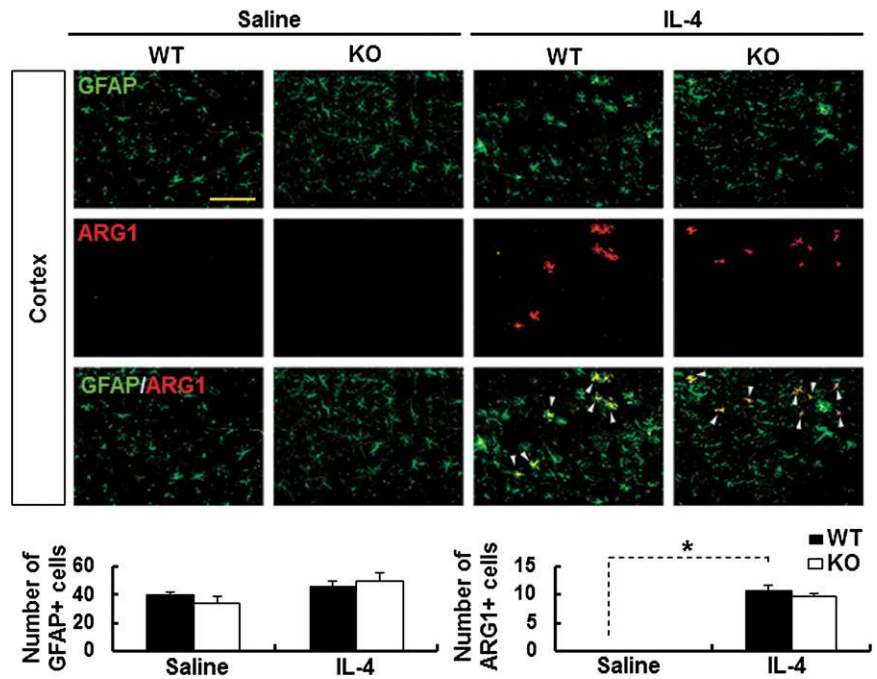
and *Megalin*) were expressed in both classically and alternatively activated astrocytes, indicating that LCN2 may act on these receptors to evoke classical activation and to inhibit alternative activation of astrocytes. In addition, injection of LPS or IL-4 into brain markedly increased the expression of classical or alternative activation-related genes, respectively, in brain astrocytes. In contrast, LPS-induced classical activation of astrocytes was notably reduced in *Lcn2*-deficient mice, indicating that LCN2 is a key regulator of astrocyte classical activation in vivo. In our immunohistochemical study, GFAP⁺ cells colocalized with LCN2 expression, indicating that i.c.v. LPS injection induced LCN2 expression in astrocytes (Fig. 9). Levels of the representative classical activation marker iNOS were also increased by LPS injection in astrocytes; however, in *Lcn2* KO mice, LPS-induced iNOS expression in astrocytes was not observed. The injection of LPS induced clas-

sical activation of astrocytes in both the hippocampus and cortex (Fig. 9), which is consistent with previous observations (37). Taken together, our results strongly support the proposition that LCN2 facilitates the classical proinflammatory activation of astrocytes.

In summary, astrocytes exhibit M1/M2-like functional polarization, and the polarized astrocytes probably play distinct roles in neuroinflammation and neurodegeneration. The secreted protein LCN2 of the lipocalin family promotes the proinflammatory phenotype of astrocytes, which suggests that LCN2 can be therapeutically targeted to modulate astrocyte phenotype and related diseases. Nevertheless, further studies are needed to elucidate the precise mechanisms responsible for astrocyte polarization and to better understand the role played by LCN2 in this process.
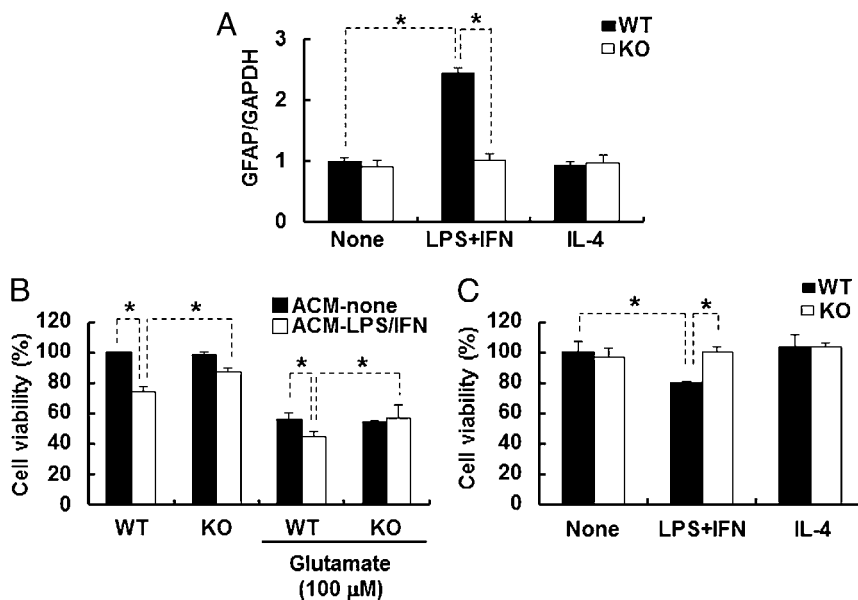

FIGURE 11. Role of LCN2 in phenotypic changes of activated astrocytes. (**A**) Primary astrocytes isolated from *Lcn2* WT or KO mice were treated with LPS (100 ng/ml) plus IFN-γ (50 U/ml) or IL-4 (10 ng/ml) for 8 h, and GFAP mRNA levels were evaluated by traditional RT-PCR using *Gapdh* as a control. (**B** and **C**) Alternatively, ACMs and astrocyte–neuron cocultures were used to assess the neurotoxic effects of activated astrocytes. After stimulating the astrocytes of WT or KO mice with LPS/IFN-γ or IL-4 for 24 h, ACMs (B) or astrocytes (in culture inserts) (C) were transferred to cortical neurons. Neuronal viabilities were measured using an MTT assay 24 h later. (B) Neurons were exposed to ACMs, with or without glutamate (100 μM), as indicated. Results are mean ± SD (*n* = 3). *$p < 0.05$. ACM-LPS/IFN, ACM after LPS (100 ng/ml)/IFN-γ (50 U/ml) treatment; ACM-none, untreated ACM.

Acknowledgments

We thank Dr. Kiyoshi Mori (Kyoto University) and Dr. Shizuo Akira (Osaka University) for generously providing the *Lcn2*-deficient mice.

Disclosures

The authors have no financial conflicts of interest.

References

1. Perea, G., M. Navarrete, and A. Araque. 2009. Tripartite synapses: astrocytes process and control synaptic information. *Trends Neurosci.* 32: 421–431.
2. Farina, C., F. Aloisi, and E. Meinl. 2007. Astrocytes are active players in cerebral innate immunity. *Trends Immunol.* 28: 138–145.
3. Sofroniew, M. V., and H. V. Vinters. 2010. Astrocytes: biology and pathology. *Acta Neuropathol.* 119: 7–35.
4. Markiewicz, I., and B. Lukomska. 2006. The role of astrocytes in the physiology and pathology of the central nervous system. *Acta Neurobiol. Exp. (Warsz.)* 66: 343–358.
5. Allan, S. M., and N. J. Rothwell. 2003. Inflammation in central nervous system injury. *Philos. Trans. R. Soc. Lond. B Biol. Sci.* 358: 1669–1677.
6. John, G. R., S. C. Lee, and C. F. Brosnan. 2003. Cytokines: powerful regulators of glial cell activation. *Neuroscientist* 9: 10–22.
7. Kim, S. U., and J. de Vellis. 2005. Microglia in health and disease. *J. Neurosci. Res.* 81: 302–313.
8. Mandrekar-Colucci, S., J. C. Karlo, and G. E. Landreth. 2012. Mechanisms underlying the rapid peroxisome proliferator-activated receptor-γ-mediated amyloid clearance and reversal of cognitive deficits in a murine model of Alzheimer's disease. *J. Neurosci.* 32: 10117–10128.
9. Xu, Y., L. Qian, G. Zong, K. Ma, X. Zhu, H. Zhang, N. Li, Q. Yang, H. Bai, J. Ben, et al. 2012. Class A scavenger receptor promotes cerebral ischemic injury by pivoting microglia/macrophage polarization. *Neuroscience* 218: 35–48.
10. David, S., and A. Kroner. 2011. Repertoire of microglial and macrophage responses after spinal cord injury. *Nat. Rev. Neurosci.* 12: 388–399.
11. Hu, X., P. Li, Y. Guo, H. Wang, R. K. Leak, S. Chen, Y. Gao, and J. Chen. 2012. Microglia/macrophage polarization dynamics reveal novel mechanism of injury expansion after focal cerebral ischemia. *Stroke* 43: 3063–3070.
12. Liu, Q., and M. Nilsen-Hamilton. 1995. Identification of a new acute phase protein. *J. Biol. Chem.* 270: 22565–22570.
13. Devireddy, L. R., C. Gazin, X. Zhu, and M. R. Green. 2005. A cell-surface receptor for lipocalin 24p3 selectively mediates apoptosis and iron uptake. *Cell* 123: 1293–1305.
14. Tong, Z., X. Wu, D. Ovcharenko, J. Zhu, C. S. Chen, and J. P. Kehrer. 2005. Neutrophil gelatinase-associated lipocalin as a survival factor. *Biochem. J.* 391: 441–448.
15. Bauer, M., J. C. Eickhoff, M. N. Gould, C. Mundhenke, N. Maass, and A. Friedl. 2008. Neutrophil gelatinase-associated lipocalin (NGAL) is a predictor of poor prognosis in human primary breast cancer. *Breast Cancer Res. Treat.* 108: 389–397.
16. Yang, J., D. Goetz, J. Y. Li, W. Wang, K. Mori, D. Setlik, T. Du, H. Erdjument-Bromage, P. Tempst, R. Strong, and J. Barasch. 2002. An iron delivery pathway mediated by a lipocalin. *Mol. Cell* 10: 1045–1056.
17. Flo, T. H., K. D. Smith, S. Sato, D. J. Rodriguez, M. A. Holmes, R. K. Strong, S. Akira, and A. Aderem. 2004. Lipocalin 2 mediates an innate immune response to bacterial infection by sequestrating iron. *Nature* 432: 917–921.
18. Wilkinson, D. G. 2001. Multiple roles of EPH receptors and ephrins in neural development. *Nat. Rev. Neurosci.* 2: 155–164.
19. Hamzic, N., A. Blomqvist, and C. Nilsberth. 2013. Immune-induced expression of lipocalin-2 in brain endothelial cells: relationship with interleukin-6, cyclooxygenase-2 and the febrile response. *J. Neuroendocrinol.* 25: 271–280.
20. Yan, Q. W., Q. Yang, N. Mody, T. E. Graham, C. H. Hsu, Z. Xu, N. E. Houstis, B. B. Kahn, and E. D. Rosen. 2007. The adipokine lipocalin 2 is regulated by obesity and promotes insulin resistance. *Diabetes* 56: 2533–2540.
21. Mori, K., H. T. Lee, D. Rapoport, I. R. Drexler, K. Foster, J. Yang, K. M. Schmidt-Ott, X. Chen, J. Y. Li, S. Weiss, et al. 2005. Endocytic delivery of lipocalin-siderophore-iron complex rescues the kidney from ischemia-reperfusion injury. *J. Clin. Invest.* 115: 610–621.
22. Lee, S., J. Lee, S. Kim, J. Y. Park, W. H. Lee, K. Mori, S. H. Kim, I. K. Kim, and K. Suk. 2007. A dual role of lipocalin 2 in the apoptosis and deramification of activated microglia. *J. Immunol.* 179: 3231–3241.
23. Naudé, P. J., C. Nyakas, L. E. Eiden, D. Ait-Ali, R. van der Heide, S. Engelborghs, P. G. Luiten, P. P. De Deyn, J. A. den Boer, and U. L. Eisel. 2012. Lipocalin 2: novel component of proinflammatory signaling in Alzheimer's disease. *FASEB J.* 26: 2811–2823.
24. Bi, F., C. Huang, J. Tong, G. Qiu, B. Huang, Q. Wu, F. Li, Z. Xu, R. Bowser, X. G. Xia, and H. Zhou. 2013. Reactive astrocytes secrete lcn2 to promote neuron death. *Proc. Natl. Acad. Sci. USA* 110: 4069–4074.
25. Ip, J. P., A. L. Noçon, M. J. Hofer, S. L. Lim, M. Müller, and I. L. Campbell. 2011. Lipocalin 2 in the central nervous system host response to systemic lipopolysaccharide administration. *J. Neuroinflammation* 8: 124.
26. Lee, S., J. Y. Park, W. H. Lee, H. Kim, H. C. Park, K. Mori, and K. Suk. 2009. Lipocalin-2 is an autocrine mediator of reactive astrocytosis. *J. Neurosci.* 29: 234–249.
27. Berard, J. L., J. G. Zarruk, N. Arbour, A. Prat, V. W. Yong, F. H. Jacques, S. Akira, and S. David. 2012. Lipocalin 2 is a novel immune mediator of experimental autoimmune encephalomyelitis pathogenesis and is modulated in multiple sclerosis. *Glia* 60: 1145–1159.
28. Rathore, K. I., J. L. Berard, A. Redensek, S. Chierzi, R. Lopez-Vales, M. Santos, S. Akira, and S. David. 2011. Lipocalin 2 plays an immunomodulatory role and has detrimental effects after spinal cord injury. *J. Neurosci.* 31: 13412–13419.
29. Dong, M., G. Xi, R. F. Keep, and Y. Hua. 2013. Role of iron in brain lipocalin 2 upregulation after intracerebral hemorrhage in rats. *Brain Res.* 1505: 86–92.
30. Marques, F., S. D. Mesquita, J. C. Sousa, G. Coppola, F. Gao, D. H. Geschwind, S. Columba-Cabezas, F. Aloisi, M. Degn, J. J. Cerqueira, et al. 2012. Lipocalin 2 is present in the EAE brain and is modulated by natalizumab. *Front Cell Neurosci* 6: 33.
31. Choi, J., H. W. Lee, and K. Suk. 2011. Increased plasma levels of lipocalin 2 in mild cognitive impairment. *J. Neurol. Sci.* 305: 28–33.
32. Chia, W. J., G. S. Dawe, and W. Y. Ong. 2011. Expression and localization of the iron-siderophore binding protein lipocalin 2 in the normal rat brain and after kainate-induced excitotoxicity. *Neurochem. Int.* 59: 591–599.
33. McCarthy, K. D., and J. de Vellis. 1980. Preparation of separate astroglial and oligodendroglial cell cultures from rat cerebral tissue. *J. Cell Biol.* 85: 890–902.
34. Kerstetter, A. E., and R. H. Miller. 2012. Isolation and culture of spinal cord astrocytes. *Methods Mol. Biol.* 814: 93–104.
35. Ock, J., H. S. Han, S. H. Hong, S. Y. Lee, Y. M. Han, B. M. Kwon, and K. Suk. 2010. Obovatol attenuates microglia-mediated neuroinflammation by modulating redox regulation. *Br. J. Pharmacol.* 159: 1646–1662.
36. Lee, S., W. H. Lee, M. S. Lee, K. Mori, and K. Suk. 2012. Regulation by lipocalin-2 of neuronal cell death, migration, and morphology. *J. Neurosci. Res.* 90: 540–550.
37. Lee, S., J. H. Kim, J. H. Kim, J. W. Seo, H. S. Han, W. H. Lee, K. Mori, K. Nakao, J. Barasch, and K. Suk. 2011. Lipocalin-2 is a chemokine inducer in the central nervous system: role of chemokine ligand 10 (CXCL10) in lipocalin-2-induced cell migration. *J. Biol. Chem.* 286: 43855–43870.
38. Cheeran, M. C., S. Hu, W. S. Sheng, P. K. Peterson, and J. R. Lokensgard. 2003. CXCL10 production from cytomegalovirus-stimulated microglia is regulated by both human and viral interleukin-10. *J. Virol.* 77: 4502–4515.
39. Park, S. Y., H. Lee, J. Hur, S. Y. Kim, H. Kim, J. H. Park, S. Cha, S. S. Kang, G. J. Cho, W. S. Choi, and K. Suk. 2002. Hypoxia induces nitric oxide production in mouse microglia via p38 mitogen-activated protein kinase pathway. *Brain Res. Mol. Brain Res.* 107: 9–16.
40. Nairz, M., I. Theurl, A. Schroll, M. Theurl, G. Fritsche, E. Lindner, M. Seifert, M. L. Crouch, K. Hantke, S. Akira, et al. 2009. Absence of functional Hfe protects mice from invasive *Salmonella enterica* serovar *Typhimurium* infection via induction of lipocalin-2. *Blood* 114: 3642–3651.
41. Qin, L., X. Wu, M. L. Block, Y. Liu, G. R. Breese, J. S. Hong, D. J. Knapp, and F. T. Crews. 2007. Systemic LPS causes chronic neuroinflammation and progressive neurodegeneration. *Glia* 55: 453–462.
42. Van Rooijen, N., and A. Sanders. 1994. Liposome mediated depletion of macrophages: mechanism of action, preparation of liposomes and applications. *J. Immunol. Methods* 174: 83–93.
43. Steel, C. D., W. K. Kim, L. D. Sanford, L. L. Wellman, S. Burnett, N. Van Rooijen, and R. P. Ciavarra. 2010. Distinct macrophage subpopulations regulate viral encephalitis but not viral clearance in the CNS. *J. Neuroimmunol.* 226: 81–92.
44. Lee, K. W., J. H. Hong, I. Y. Choi, Y. Che, J. K. Lee, S. D. Yang, C. W. Song, H. S. Kang, J. H. Lee, J. S. Noh, et al. 2002. Impaired D2 dopamine receptor function in mice lacking type 5 adenylyl cyclase. *J. Neurosci.* 22: 7931–7940.
45. Castagne, V., P. Moser, S. Roux, and R. D. Porsolt. 2011. Rodent models of depression: forced swim and tail suspension behavioral despair tests in rats and mice. *Curr. Protoc. Neurosci.* Chapter 8: Unit 8.10A.
46. Lee, S., E. Jang, J. H. Kim, J. H. Kim, W. H. Lee, and K. Suk. 2012. Lipocalin-type prostaglandin D2 synthase protein regulates glial cell migration and morphology through myristoylated alanine-rich C-kinase substrate: prostaglandin D2-independent effects. *J. Biol. Chem.* 287: 9414–9428.
47. Jang, E., S. Lee, J. H. Kim, J. H. Kim, J. W. Seo, W. H. Lee, K. Mori, K. Nakao, and K. Suk. 2013. Secreted protein lipocalin-2 promotes microglial M1 polarization. *FASEB J.* 27: 1176–1190.
48. Sofroniew, M. V. 2009. Molecular dissection of reactive astrogliosis and glial scar formation. *Trends Neurosci.* 32: 638–647.
49. Zhou, F., H. H. Yao, J. Y. Wu, Y. J. Yang, J. H. Ding, J. Zhang, and G. Hu. 2006. Activation of Group II/III metabotropic glutamate receptors attenuates LPS-induced astroglial neurotoxicity via promoting glutamate uptake. *J. Neurosci. Res.* 84: 268–277.
50. McNaught, K. S., and P. Jenner. 2000. Extracellular accumulation of nitric oxide, hydrogen peroxide, and glutamate in astrocytic cultures following glutathione depletion, complex I inhibition, and/or lipopolysaccharide-induced activation. *Biochem. Pharmacol.* 60: 979–988.
51. Bluthé, R. M., J. Lestage, G. Rees, A. Bristow, and R. Dantzer. 2002. Dual effect of central injection of recombinant rat interleukin-4 on lipopolysaccharide-induced sickness behavior in rats. *Neuropsychopharmacology* 26: 86–93.
52. Hvidberg, V., C. Jacobsen, R. K. Strong, J. B. Cowland, S. K. Moestrup, and N. Borregaard. 2005. The endocytic receptor megalin binds the iron transporting neutrophil-gelatinase-associated lipocalin with high affinity and mediates its cellular uptake. *FEBS Lett.* 579: 773–777.
53. Mantovani, A., S. Sozzani, M. Locati, P. Allavena, and A. Sica. 2002. Macrophage polarization: tumor-associated macrophages as a paradigm for polarized M2 mononuclear phagocytes. *Trends Immunol.* 23: 549–555.
54. O'Shea, J. J., M. Pesu, D. C. Borie, and P. S. Changelian. 2004. A new modality for immunosuppression: targeting the JAK/STAT pathway. *Nat. Rev. Drug Discov.* 3: 555–564.

55. Ridet, J. L., S. K. Malhotra, A. Privat, and F. H. Gage. 1997. Reactive astrocytes: cellular and molecular cues to biological function. *Trends Neurosci.* 20: 570–577.

56. Matyash, V., and H. Kettenmann. 2010. Heterogeneity in astrocyte morphology and physiology. *Brain Res. Brain Res. Rev.* 63: 2–10.

57. Chaboub, L. S., and B. Deneen. 2012. Developmental origins of astrocyte heterogeneity: the final frontier of CNS development. *Dev. Neurosci.* 34: 379–388.

58. McKhann, G. M., II, R. D'Ambrosio, and D. Janigro. 1997. Heterogeneity of astrocyte resting membrane potentials and intercellular coupling revealed by whole-cell and gramicidin-perforated patch recordings from cultured neocortical and hippocampal slice astrocytes. *J. Neurosci.* 17: 6850–6863.

59. Olsen, M. L., S. L. Campbell, and H. Sontheimer. 2007. Differential distribution of Kir4.1 in spinal cord astrocytes suggests regional differences in K+ homeostasis. *J. Neurophysiol.* 98: 786–793.

60. Israel, J. M., C. G. Schipke, C. Ohlemeyer, D. T. Theodosis, and H. Kettenmann. 2003. GABAA receptor-expressing astrocytes in the supraoptic nucleus lack glutamate uptake and receptor currents. *Glia* 44: 102–110.

61. Wallraff, A., B. Odermatt, K. Willecke, and C. Steinhäuser. 2004. Distinct types of astroglial cells in the hippocampus differ in gap junction coupling. *Glia* 48: 36–43.

62. Regan, M. R., Y. H. Huang, Y. S. Kim, M. I. Dykes-Hoberg, L. Jin, A. M. Watkins, D. E. Bergles, and J. D. Rothstein. 2007. Variations in promoter activity reveal a differential expression and physiology of glutamate transporters by glia in the developing and mature CNS. *J. Neurosci.* 27: 6607–6619.

63. Pivneva, T., B. Haas, D. Reyes-Haro, G. Laube, R. W. Veh, C. Nolte, G. Skibo, and H. Kettenmann. 2008. Store-operated Ca2+ entry in astrocytes: different spatial arrangement of endoplasmic reticulum explains functional diversity in vitro and in situ. *Cell Calcium* 43: 591–601.

64. Emsley, J. G., and J. D. Macklis. 2006. Astroglial heterogeneity closely reflects the neuronal-defined anatomy of the adult murine CNS. *Neuron Glia Biol.* 2: 175–186.

65. Bachoo, R. M., R. S. Kim, K. L. Ligon, E. A. Maher, C. Brennan, N. Billings, S. Chan, C. Li, D. H. Rowitch, W. H. Wong, and R. A. DePinho. 2004. Molecular diversity of astrocytes with implications for neurological disorders. *Proc. Natl. Acad. Sci. USA* 101: 8384–8389.

66. Doyle, J. P., J. D. Dougherty, M. Heiman, E. F. Schmidt, T. R. Stevens, G. Ma, S. Bupp, P. Shrestha, R. D. Shah, M. L. Doughty, et al. 2008. Application of a translational profiling approach for the comparative analysis of CNS cell types. *Cell* 135: 749–762.

67. Brahmachari, S., Y. K. Fung, and K. Pahan. 2006. Induction of glial fibrillary acidic protein expression in astrocytes by nitric oxide. *J. Neurosci.* 26: 4930–4939.

68. Mizuno, T., R. Kuno, A. Nitta, T. Nabeshima, G. Zhang, J. Kawanokuchi, J. Wang, S. Jin, H. Takeuchi, and A. Suzumura. 2005. Protective effects of nicergoline against neuronal cell death induced by activated microglia and astrocytes. *Brain Res.* 1066: 78–85.

69. Zeng, K. W., T. Zhang, H. Fu, G. X. Liu, and X. M. Wang. 2012. Modified Wu-Zi-Yan-Zong prescription, a traditional Chinese polyherbal formula, suppresses lipopolysaccharide-induced neuroinflammatory processes in rat astrocytes via NF-κB and JNK/p38 MAPK signaling pathways. *Phytomedicine* 19: 122–129.

70. von Boyen, G. B., M. Steinkamp, M. Reinshagen, K. H. Schäfer, G. Adler, and J. Kirsch. 2004. Proinflammatory cytokines increase glial fibrillary acidic protein expression in enteric glia. *Gut* 53: 222–228.

71. Derecki, N. C., A. N. Cardani, C. H. Yang, K. M. Quinnies, A. Crihfield, K. R. Lynch, and J. Kipnis. 2010. Regulation of learning and memory by meningeal immunity: a key role for IL-4. *J. Exp. Med.* 207: 1067–1080.

72. Bélanger, M., I. Allaman, and P. J. Magistretti. 2011. Differential effects of pro- and anti-inflammatory cytokines alone or in combinations on the metabolic profile of astrocytes. *J. Neurochem.* 116: 564–576.

73. Koeberle, P. D., J. Gauldie, and A. K. Ball. 2004. Effects of adenoviral-mediated gene transfer of interleukin-10, interleukin-4, and transforming growth factor-beta on the survival of axotomized retinal ganglion cells. *Neuroscience* 125: 903–920.

74. Brodie, C., N. Goldreich, T. Haiman, and G. Kazimirsky. 1998. Functional IL-4 receptors on mouse astrocytes: IL-4 inhibits astrocyte activation and induces NGF secretion. *J. Neuroimmunol.* 81: 20–30.

75. Ahn, M., C. Lee, K. Jung, H. Kim, C. Moon, K. B. Sim, and T. Shin. 2012. Immunohistochemical study of arginase-1 in the spinal cords of rats with clip compression injury. *Brain Res.* 1445: 11–19.

76. Garg, S. K., J. Kipnis, and R. Banerjee. 2009. IFN-gamma and IL-4 differentially shape metabolic responses and neuroprotective phenotype of astrocytes. *J. Neurochem.* 108: 1155–1166.

77. Park, S. J., J. H. Lee, H. Y. Kim, Y. H. Choi, J. S. Park, Y. H. Suh, S. M. Park, E. H. Joe, and I. Jou. 2012. Astrocytes, but not microglia, rapidly sense H$_2$O$_2$ via STAT6 phosphorylation, resulting in cyclooxygenase-2 expression and prostaglandin release. *J. Immunol.* 188: 5132–5141.

78. Tarassishin, L., O. Loudig, A. Bauman, B. Shafit-Zagardo, H. S. Suh, and S. C. Lee. 2011. Interferon regulatory factor 3 inhibits astrocyte inflammatory gene expression through suppression of the proinflammatory miR-155 and miR-155*. *Glia* 59: 1911–1922.

79. Li, C., and Y. R. Chan. 2011. Lipocalin 2 regulation and its complex role in inflammation and cancer. *Cytokine* 56: 435–441.

80. Cowland, J. B., O. E. Sørensen, M. Sehested, and N. Borregaard. 2003. Neutrophil gelatinase-associated lipocalin is up-regulated in human epithelial cells by IL-1 beta, but not by TNF-alpha. *J. Immunol.* 171: 6630–6639.

81. Zamanian, J. L., L. Xu, L. C. Foo, N. Nouri, L. Zhou, R. G. Giffard, and B. A. Barres. 2012. Genomic analysis of reactive astrogliosis. *J. Neurosci.* 32: 6391–6410.